

TU Dortmund University

Faculty of Statistics



Analysis of Orientations of Micro Cracks via Circular Statistics

Bachelor Thesis

by

Katja Falta

Supervisor: Prof. Dr. Christine H. Müller

Submission Date: July 21st, 2011

Contents

- 1 Introduction** **1**

- 2 Problem** **2**

- 3 Experimental Procedure** **4**

- 4 Data** **5**

- 5 Statistical Methods** **7**
 - 5.1 Graphical Representation 8
 - 5.1.1 Circular Raw Data Plot 8
 - 5.1.2 Histogram 9
 - 5.1.3 Rose Diagram 10
 - 5.2 Measures of Location, Concentration and Dispersion 10
 - 5.2.1 Preliminaries and Notation 12
 - 5.2.2 Mean Resultant Length 13
 - 5.2.3 Circular Mean Direction 14
 - 5.2.4 Circular Median Direction 15
 - 5.2.5 Sample Circular Variance 15
 - 5.2.6 Circular Standard Deviation 15
 - 5.2.7 Circular Range 16

- 6 Statistical Analysis** **16**
 - 6.1 Computation of the Angles 16
 - 6.2 Crack Analysis of Specimen 10 17
 - 6.2.1 Orientation at Initial Stage 20
 - 6.2.2 Orientation at Stable Propagation Stage 22
 - 6.3 Crack Analysis of Specimen 31 24
 - 6.3.1 Orientation at Initial Stage 26
 - 6.3.2 Orientation at Stable Propagation Stage 28
 - 6.4 Comparison between Specimen 10 and Specimen 31 29

- 7 Conclusion** **34**

A Appendix	36
A.1 Plots	36
A.2 Tables	40
A.3 R-Codes	46
B References	52
Eidesstattliche Erklärung des Urhebers	53

1 Introduction

Steel is one of the most widely-used materials in the world due to its versatility. Its properties, including hardness, ductility and tensile strength, are important to industries such as engineering and architecture. Although steel is very robust, cracks do occur under too much stress applied to it. The understanding of crack initiation and crack growth is very important, e.g. for predicting the life time of products like wheels of trains or hip replacement. Thus, it is crucial to know the significant characteristics of steel like its behavior under stress and how this effects the life time of the material. Therefore, many experiments are performed to examine how and when cracks occur and propagate. This is often done by applying fatigue loading.

In this paper, a closer look is taken at data that were acquired during standard fatigue experiments performed at the University of Kassel, Germany, where the relationship between load cycles and crack behavior in steel was investigated. The focus is set on two different specimens of low carbon steel. While stress was applied to them, images were taken with a long-distance microscope at different time points of the fatigue process. Those pictures were then used to gain information of the cracks' development along the increasing number of load cycles. The data sets used in the following analysis contain information of each specimen at each point of time. The variables considered are the lengths of the cracks paths, the sizes of the crack clusters, and the x - and y -coordinates of the start and end points of the crack paths. Of interest is the crack orientation in each of those two assays.

The underlying development of cracks is already known. According to Besel and Brückner-Foit (2008), a general damage accumulation consists of three stages, namely crack initiation, small crack propagation and stable crack propagation of long cracks. Especially, the latter two phases are the ones to be examined in terms of two hypotheses. The first one is that micro cracks have an orientation with an angle of about 45° or 135° with respect to the loading axis as they begin to grow. The second hypothesis refers to the third stage. Fact is that eventually, i.e. after a certain number of load cycles has been applied to the material, most micro cracks merge, forming long cracks. The hypothesis is that those so-called macro cracks propagate perpendicular to the stress. Another aspect to be analyzed in this paper is to find out whether it is possible to distinguish between two specimens that obtained different stress levels at an early stage of the fatigue load-

ing process. This is examined by comparing the crack orientations in both specimens per number of load cycles.

Since it is dealt with orientations, using linear statistics is inappropriate. Special directional methods need to be applied in order to properly characterize the angular observations. Due to the fact that circular data arise in many scientific areas, e.g. Earth Sciences, Meteorology, Biology, Physics, Psychology, Image Analysis, Medicine, Astronomy, the analysis of such information has become more and more important over the last decades (Mardia and Jupp, 2000, pp. 7). Some basic statistical tools used in circular statistics, such as the calculation of measures of location and dispersion, are applied to both data sets in order to verify or to disprove the hypotheses.

The paper is organized as follows. Section 2 specifies the aim of the analysis conducted and the problems that arise when handling circular data. In Section 3 the experimental procedure is explained, which is followed by a detailed description of the data sets in Section 4. Thereafter, the statistical methods commonly used in circular statistics will be provided in Section 5. The statistical analysis can be found in Section 6. While both specimens are analyzed individually in Subsections 6.2 and 6.3, the two are compared with one another in Subsection 6.4. Finally, a discussion of the results, a conclusion and an outlook are given in Section 7.

2 Problem

Cracks can roughly be distinguished between micro and macro cracks. The latter ones originate from micro cracks, which in turn arise from plastic deformations of the material and are so tiny that they are only visible with the help of a microscope (Gunkel et al., 2011). Since micro cracks are always surrounded by plastic deformations, it is not seldom difficult to tell the difference between them. However, they do differ in color, i.e. cracks are darker, and hence, the crack paths in those so-called crack clusters can be determined by following their darkest parts. To obtain only one main path per cluster is very important, since their lengths are most relevant for the stability of the material, Gunkel et al. (2011) point out.

There already exist several ways for determining cracks. A common method is to describe crack clusters as ellipses or rectangles and to define the lengths of their main axes

as the cracks' lengths. Since this approximation only considers the start and end points of the paths, but not its kinks and curves, it is not a very good approach. Also, skeletonization and thinning methods are only slightly better approaches. Therefore, Gunkel et al. (2011) developed an R package called `crackrec`, which provides an improved way of detecting and analyzing micro cracks. This package was used to identify all cracks in the low carbon steel assays, which are examined in this paper. An example is given in Figure 1, where an image segment of one of the two specimens is shown. The original image is given on the left hand side. On the right hand side, all cracks detected by `crackrec` are added to the plot. The red lines denote the crack paths and the yellow lines connect the start and end points of each crack.

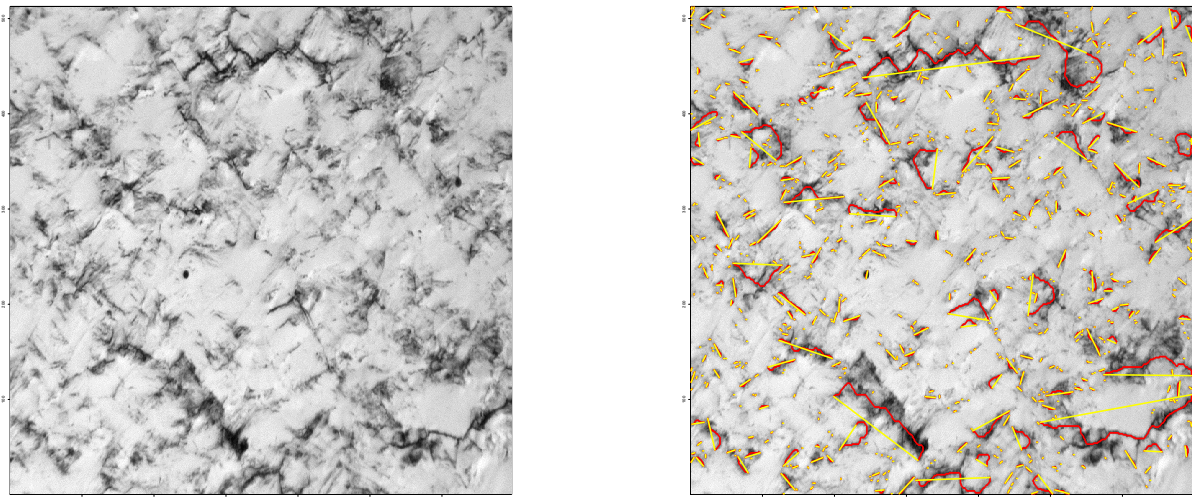


Figure 1: Image segment of Specimen 31. Left: original image after 18000 load cycles; Right: detected cracks in that image

The data sets available consist of information of two steel specimens that were exposed to stress and as a result developed cracks. During the experiments, hundreds of images were taken of the assays' surfaces. With the help of the statistical software R (R Development Core Team, 2009) and the package `crackrec`, the images were then used to identify the cracks. The information gained are utilized to examine the cracks' behavior, especially, how they behave when gradually more stress is applied.

The main focus of the analysis conducted was to investigate two assumptions. First, to check whether micro cracks have an orientation with an angle of about 45° or 135° with respect to the loading axis in the initial stage. Second, to find out whether the orientations of the cracks are tending to be perpendicular to the stress after the micro cracks have

become macro cracks. Those two theses are checked by looking at each specimen individually. However, it is reasonable to compare both of them with one another to see how the behavior of the cracks resembles or differs. This raised another interesting question, namely whether it is possible to tell the difference between an assay exposed to a lower stress level and an assay exposed to a higher stress level at an early stage of the damage evolution. If this is feasible just by analyzing the orientations of the cracks, it would mean that it is sufficient to only look at one image segment instead of a specimen's composed total image.

Since orientations describe directions and are given as either coordinates or angles, linear statistical analysis can not be applied. As a result of that, a special branch of statistics is used: circular statistics. Consequently, different statistical methods are required for carrying out the analysis. Those methods are explained in Section 5.

3 Experimental Procedure

The data to be analyzed were obtained via standard fatigue experiments performed on a servohydraulic testing machine (Besel and Brückner-Foit, 2008). On hand are information of two assays, hereinafter referred to as Specimen 10 and Specimen 31, that were exposed to different stress levels. While a nominal stress level of 400 MPa was applied to Specimen 31, Specimen 10 obtained a stress level of 360 MPa (Müller et al., 2011). The round specimens examined were composed of low carbon steel, German designation 51CrV4, having a length of 115 mm and a main diameter of 12 mm (Müller et al., 2011). In order to investigate the initiation and growth of the fatigue cracks, it is sufficient to focus only on the central part of the test pieces. Hence, a length of 19 mm was symmetrically notched in the middle of the specimens reducing the diameter to 7.6 mm and to 7 mm in the inner part with a length of 10 mm (Müller et al., 2011). By flattening the two opposite sides of the round inner part, the distance between those sides was shortened to 6 mm (Müller et al., 2011).

Besel and Brückner-Foit (2008) mention that the experiments included standard tension tests and hardness tests and that fully reversed loading was applied at room temperature. To facilitate surface observation, both assays were grounded and polished before the experiments started (Besel and Brückner-Foit, 2008). With a working distance of 46

mm the surfaces were scanned after predefined numbers of load cycles via a long-distance microscope (Hirox, Japan) (Besel and Brückner-Foit, 2008). With a 1.14 MPig b/w camera, which was set up on a three-axis stage in front of the testing machine, hundreds of images of each specimen were taken, which provided the basis for obtaining the data used in this paper (Besel and Brückner-Foit, 2008).

4 Data

The aim of the fatigue experiments performed was to “observe the damage evolution as a function of the number of load cycles” (Besel and Brückner-Foit, 2008). Thus, each specimen’s surface was scanned after predefined time points given by the number of load cycles. While there were 29 different points of time for Specimen 10, 15 time points were considered for Specimen 31. More precisely, images of Specimen 10 were taken “at the beginning and in steps of 1000 load cycles up to 20000 load cycles and then after 25000, 30000, 35000, 37000, 39000, 40000, 42000, and 44000 load cycles” and images of Specimen 31 were obtained “at the beginning and after 1000, 2000, 3000, 4000, 5000, 5000, 7000, 8000, 9000, 10000, 12000, 14000, 16000, 18000 load cycles” (Müller et al., 2011).

According to Müller et al. (2011), the images were taken from an area of about 4×5 mm² size lying on the flat part of the specimen, and since this was too large to cover with a single picture, the photo had to be divided into segments. Ultimately, there were $9 \times 5 = 45$ image segments and $9 \times 6 = 54$ image segments for Specimen 10 and Specimen 31, respectively, where one image segment consists of 696×512 pixels and 80 pixels correspond to 100 μ m (Müller et al., 2011). Total images of Specimen 10 with 2659×4221 pixels and of Specimen 31 with 3337×4165 pixels were attained by joining their segments (Müller et al., 2011). For a faster analysis the images were compressed by 50%, such that the total images of Specimen 10 and Specimen 31 have a size of 1330×2111 and 1669×2083 pixels, respectively (Müller et al., 2011). It is to note that the quality of the segments differ, i.e. some of them are blurred or contain shadows at the border (Müller et al., 2011). Composed total images of Specimen 10 and Specimen 31 before and after the experiment are shown in Figures 2 and 3, respectively.

The images obtained are analyzed by using the free statistical software R (R Development Core Team, 2009). One very helpful package provided by R is `crackrec`, which

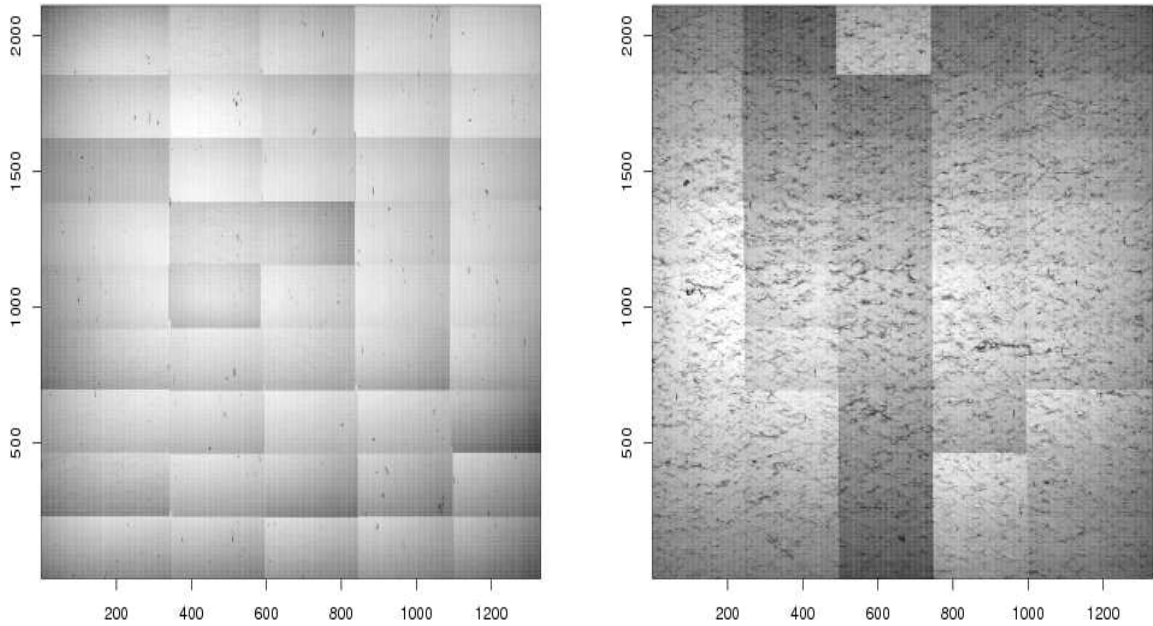


Figure 2: Composed total image of Specimen 10. Left: 0 load cycles; Right: 44000 load cycles

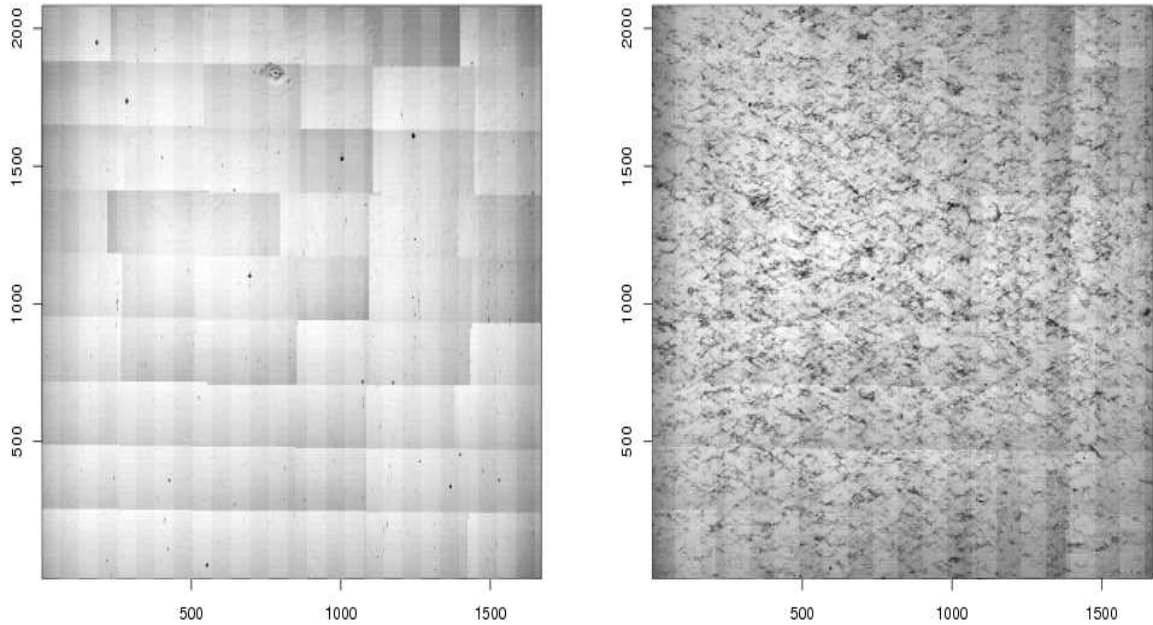


Figure 3: Composed total image of Specimen 31. Left: 0 load cycles; Right: 18000 load cycles

was introduced by Gunkel et al. (2011). It allows an automatic detection of micro cracks and a statistical analysis of crack quantities (Gunkel et al., 2011). Via the function `rbmp`, the images can be converted from bmp files to R data sets. Furthermore, `crackrec` includes a function called `median.filter`, which removes the shadows in the images. In the following analysis a median filter with a window of 101×101 was used.

Another function included in the package is `crackrec`, which “provides the cracks from a gray level image matrix” and its output consists of three components, namely `crackclusters`, `crackpaths` and `cracks` (Gunkel et al., 2011). The latter one provides the data sets used in this paper. More precisely, for each specimen and time point information are listed in a $6 \times K$ matrix, where K denotes the number of crack clusters found (Gunkel et al., 2011). The six rows contain the lengths of the cracks paths (`length`), the sizes of the crack clusters (`size`) and the x - and y -coordinates of the start and end points of the crack paths (`Begin_x`, `Begin_y`, `End_x`, `End_y`). The variables `length` and `size` are given in pixels, where 1 pixel corresponds to $2.5 \mu\text{m}$.

5 Statistical Methods

Circular data are observations that are measured in angles or that are two-dimensional orientations (Fisher, 1993, p. xv). In other words, the measurements are directions (Jammalamadaka and SenGupta, 2001, p. 1). Two principal measuring instruments closely associated with angular data are the compass and the clock (Mardia and Jupp, 2000, p. 1). Jammalamadaka and SenGupta (2001, p. 1) note that a direction has no magnitude, which allows a representation on the circumference of the unit circle centered at the origin or as a unit vector connecting the origin to that point. It is usual to measure circular data in degrees, although it is sometimes advantageous to convert the degrees to radians by multiplying them by $\frac{\pi}{180}$ (Mardia and Jupp, 2000, p. 1).

In order to specify an angle, it is necessary to determine an appropriate zero-direction, which means to choose a starting point and a sense of rotation (clockwise or anti-clockwise) as the positive direction (Jammalamadaka and SenGupta, 2001, p. 1). The importance of providing these information can be illustrated by considering the following example. A mathematician commonly regards East as the zero-direction and anti-clockwise as the positive direction, but to other scientists, for instance Geologists, the zero-direction is

often North and the positive direction is defined to be clockwise. As a result, an angle of 60° looked at by a mathematician would be called an angle of 30° by a Geologist, see Figure 4 (based on a plot in Jammalamadaka and SenGupta (2001, p. 2)). For the analysis conducted in this paper the zero-direction is East and the sense of rotation is anti-clockwise.

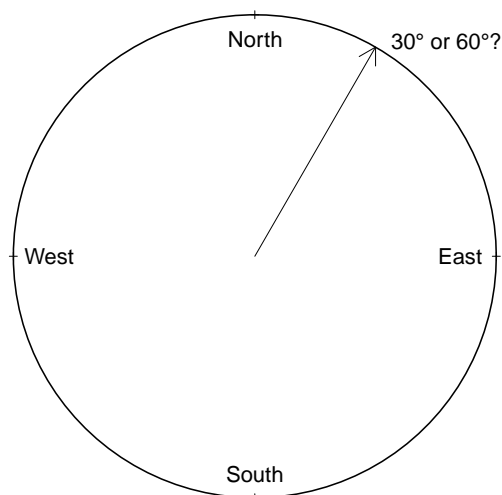


Figure 4: Value depends on choice of origin and sense of orientation

Another important feature of angular data to keep in mind is the fact that the ‘beginning’ of the circle is also the ‘end’, i.e. $0 = 2\pi$, and that “the measurement is periodic with θ being the same as $\theta + p \cdot 2\pi$ for any integer p ” (Jammalamadaka and SenGupta, 2001, p. 2). Among other things, these are the reasons why the analysis of circular data is different from a linear statistical analysis. Some of the main statistical methods for circular data, which are used in this paper, are presented below.

5.1 Graphical Representation

To gain a first idea of the circular data given, it is advisable to visually depict them. There are a few useful plots to accomplish this.

5.1.1 Circular Raw Data Plot

A circular raw data plot is the most basic form of representing circular data by displaying each observation as a point on the unit circle (Mardia and Jupp, 2000, p. 1). Those data

points can either be stacked on the outside of the circle or they can be plotted on the circle's perimeter. Stacking is indicated, when the observations are closely distributed, because information might get lost, if the data points are overplotted. The big advantage of a circular raw data plot is that it can help to get a first impression of whether the data contain special characteristics such as modal groups or outliers (Fisher, 1993, p. 16).

Figure 5 shows two circular raw data plots of the initial directions taken by 76 turtles, which were released after treatment (Stephens, 1969). The aim of the experiment performed was to examine whether the turtles have a preferred direction. Especially, the plot on the left hand side in Figure 5 supports this assumption. A list of all 76 observations can be found in the Appendix A.2, Table 14.

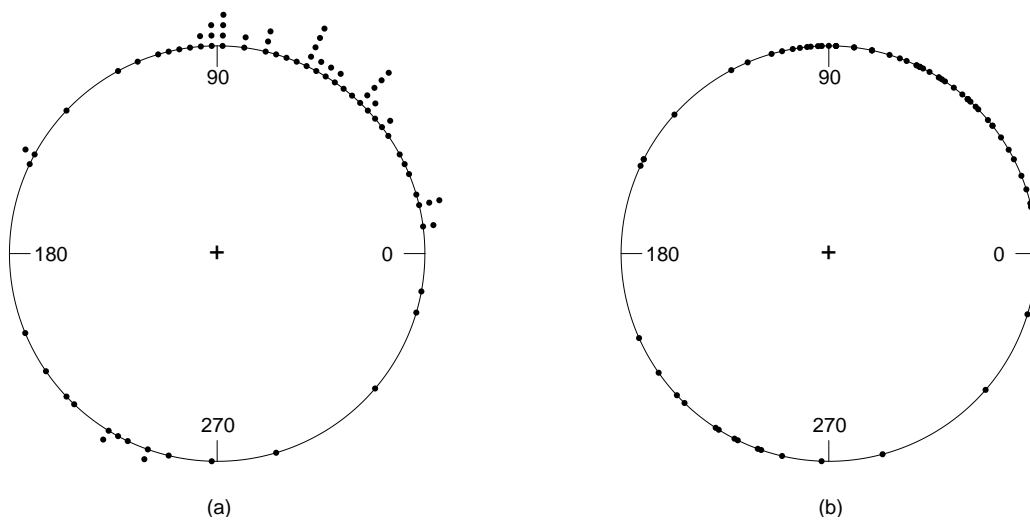


Figure 5: Orientations of 76 turtles: (a) stacked (b) not stacked

5.1.2 Histogram

Another way of representing directional data is to graph a histogram. This is essentially constructed by grouping the observations into intervals, which is then followed by summing them up within each group and displaying the resulting frequencies as bars or bins. There exist two types of histograms for circular data, angular and linear (Fisher, 1993, p. 17).

Angular: In a circular histogram, all angles between 0° and 360° are divided into intervals, such that each observation falls into one of the groups. A group's relative frequency determines the length of the bar. The area of a bar is proportional to the

frequency in that group and all bars are centered at the midpoint of the corresponding group (Mardia and Jupp, 2000, p. 2). This kind of plot is useful for visualizing the frequencies with which the data occur relative to the values, that is whether the frequency is consistent over the range or concentrated at some value.

Linear: Another possibility is to represent the measured directions in a linear histogram, which again gives a rough approximation of the frequency distribution. The advantage is that statisticians are more experienced with the interpretation of histograms on the real line (Mardia and Jupp, 2000, p. 2).

It is worth mentioning that an angular histogram can be obtained from a linear histogram and vice versa. This is achieved by wrapping a linear histogram around a circle creating the angular histogram, or by cutting the circular histogram at a suitably chosen point on the circle and then unrolling it to a linear histogram on an interval of width 360° (Fisher, 1993, p. 17; Mardia and Jupp, 2000, p. 2).

Note that both types of histograms are sensitive to the intervals chosen, and that the visual impression given by a linear histogram can differ depending on the point at which the circle is cut (Mardia and Jupp, 2000, p. 2).

5.1.3 Rose Diagram

The rose diagram is a special type of angular histogram. The main difference is that the bars are substituted by sectors, each still representing a group (Mardia and Jupp, 2000, p. 4). According to Fisher (2011, p. 18), each sector's radius should be proportional to the square root of the relevant frequency when the grouping is equidistant. This ensures that each sector's area is proportional to the group frequency, Mardia and Jupp (2000, p. 4) add. Naturally, the number of sectors present in the plot is equal to the number of groups.

5.2 Measures of Location, Concentration and Dispersion

Once the circular data have been plotted, it is advisable to calculate some summary statistics. These provide further help to characterize the sample given and to gain a better idea of how the data are distributed.

When dealing with circular data, the main thing of interest is whether there exists a preferred direction. Intuitively, it makes sense to calculate the mean direction of all observations available. However, since the data are angular, it is inappropriate to simply use the arithmetic mean, i.e. to sum up all angles and to divide that sum by the number of angles observed. Consider for instance the following example presented by Jammalamadaka and SenGupta (2001, p. 11), which is visualized in Figure 6. Assume there is one bird flying at 15° and another bird flying at 345° . When taking East as the zero direction and anti-clockwise as the positive sense of rotation, it is obvious to state that both observations point towards East. On the other hand, if the arithmetic mean is calculated, $\frac{1}{2}(15^\circ + 345^\circ) = 180^\circ$, the observations point towards West, which is apparently not the case.

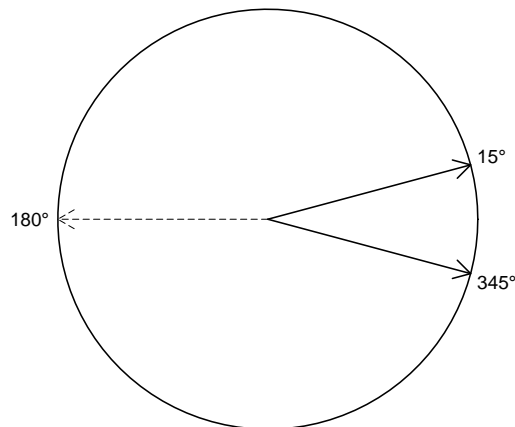


Figure 6: Arithmetic mean of two directions

In order to avoid this kind of problem, the mean direction of circular data is calculated differently. All observations are treated as unit vectors and then the direction of their resultant vector is used. Let's look at another example to clarify the importance of this procedure.

Given are three directions, which can be seen on the left hand of Figure 7. When taking East as the zero-direction and anti-clockwise as the sense of rotation, these angles are by name 0° , 45° and 315° . The resultant vector is obtained by combining all vectors via common vector addition, which is shown on the right hand side of Figure 7.

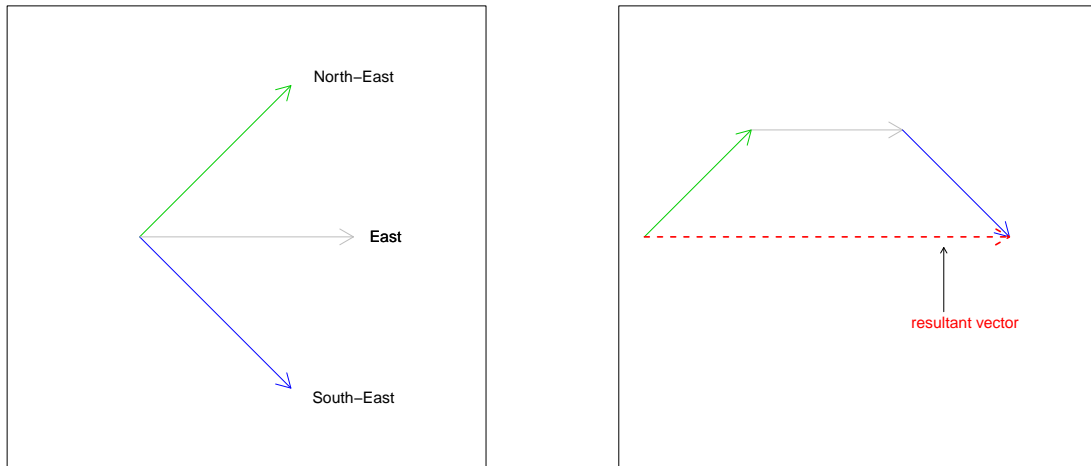


Figure 7: Three directions. Left: vectors representing the observations; Right: vector addition

This vector describes the average direction of all vectors. If the length of the resultant vector is divided by the number of vectors, see left hand side of Figure 8, a vector with a length in the range of 0 and 1 is obtained, which is the resulting mean vector. Its length is an indicator for the variability of the observed directions. In other words, the bigger the value, the more point all angles towards the same direction, see the right hand side of Figure 8.

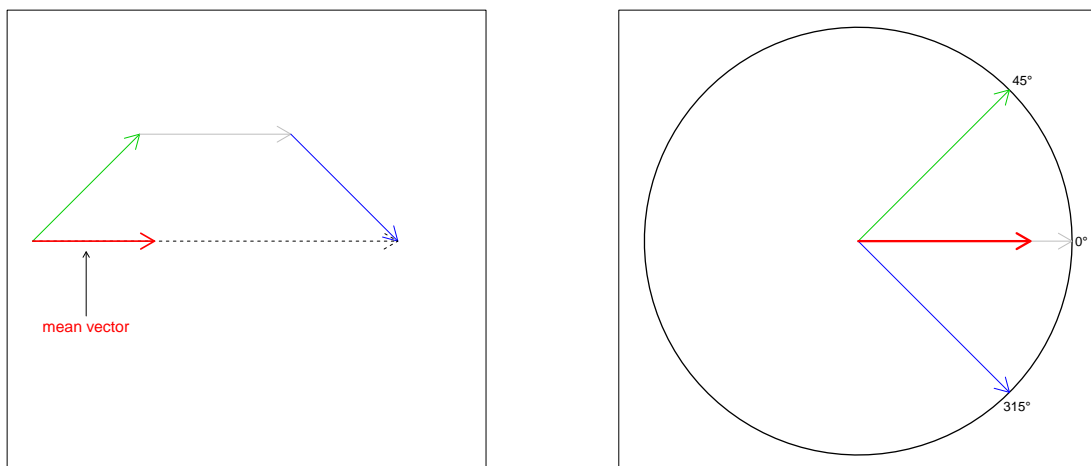


Figure 8: Three directions. Left: mean vector; Right: mean direction added to unit circle

5.2.1 Preliminaries and Notation

As explained earlier, circular data can be represented as points on the circumference on the unit circle. Thus, the directional position can be uniquely determined by two coordinates, the x - and the y -coordinate (Jammalamadaka and SenGupta, 2001, p. 9). Those so-called

Cartesian coordinates can easily be converted to polar coordinates and vice versa by using trigonometric functions. Consider a point with polar coordinates (r, θ) , where r denotes the distance to the origin and θ denotes the direction (Jammalamadaka and SenGupta, 2001, p. 9). Then the two coordinate systems are related by the following equations:

$$x = r \cdot \cos \theta , \quad y = r \cdot \sin \theta .$$

This relation is illustrated in Figure 9. Obviously, $r = 1$ when dealing with the unit circle.

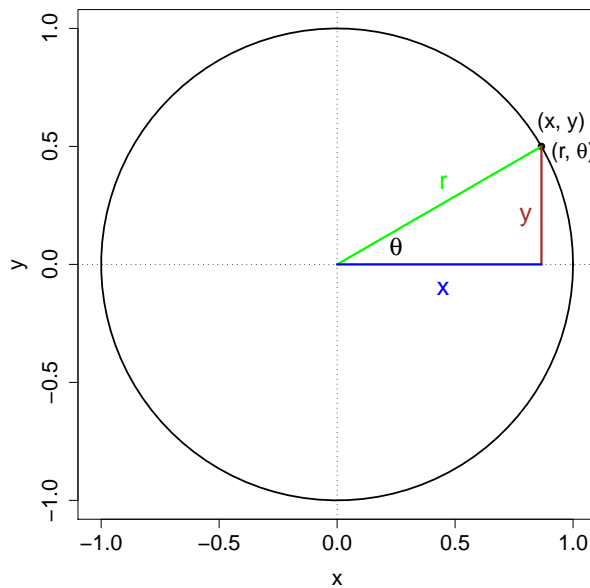


Figure 9: Relation between Cartesian and polar coordinates

Remember that θ and $\theta + 360^\circ$, or alternatively θ and $\theta + 2\pi$, describe the same point on the circle, provided that the angles are measured in degrees or radians, respectively. Hence, in the following analysis all arithmetic done will be modulo 360° or modulo 2π .

5.2.2 Mean Resultant Length

In order to determine the resultant length, the *resultant vector* \mathbf{R} needs to be obtained. Jammalamadaka and SenGupta (2001, p. 11) explain that this is accomplished by summing the coordinates of all n unit vectors component-wise

$$\mathbf{R} = \left(\sum_{j=1}^n \cos \theta_j , \sum_{j=1}^n \sin \theta_j \right) = (C, S) .$$

Consequently, the length of this vector is the *resultant length* R and can be calculated via Pythagoras' theorem

$$R = \sqrt{C^2 + S^2} .$$

Apparently, the value of R has to lie in the range of $(0, n)$ (Fisher, 1993, p. 32). The *mean resultant length* \bar{R} is given by

$$\bar{R} = \frac{R}{n} ,$$

where $0 \leq \bar{R} \leq 1$ (Mardia and Jupp, 2000, p. 17). According to Mardia and Jupp (2000, pp. 17), \bar{R} will be close to 1, if $\theta_1, \dots, \theta_n$ are tightly clustered, but it will be almost 0, if the directions are widely dispersed. Fisher (1993, p. 32) further points out, $\bar{R} = 1$ means that all data points are coincident, yet " $\bar{R} = 0$ does not imply uniform distribution around the circle". That is why the mean resultant length is a measure of concentration. Note also that \bar{R} is invariant under rotation (Mardia and Jupp, 2000, p. 18).

The mean resultant length for the example given at the beginning of this subsection is $\bar{R} = \frac{1}{3} \cdot \sqrt{[\cos(0^\circ) + \cos(45^\circ) + \cos(315^\circ)]^2 + [\sin(0^\circ) + \sin(45^\circ) + \sin(315^\circ)]^2} = 0.8047$.

5.2.3 Circular Mean Direction

The *circular mean direction* $\bar{\theta}$ is given by the direction of the resultant vector and it can be calculated in two different ways, Jammalamadaka and SenGupta (2001, p. 13) explain. Either by finding a solution to the equations

$$\cos \bar{\theta} = \frac{C}{R} \quad \text{and} \quad \sin \bar{\theta} = \frac{S}{R}$$

or by applying the following case distinction

$$\bar{\theta} = \begin{cases} \tan^{-1} \left(\frac{S}{C} \right) , & \text{if } C > 0, S \geq 0 , \\ \tan^{-1} \left(\frac{S}{C} \right) + \pi , & \text{if } C < 0 , \\ \tan^{-1} \left(\frac{S}{C} \right) + 2\pi , & \text{if } C \geq 0, S < 0 , \\ \frac{\pi}{2} , & \text{if } C = 0, S > 0 , \\ \text{not defined} , & \text{if } C = 0, S = 0 . \end{cases} \quad (1)$$

Jammalamadaka and SenGupta (2001, p. 13) point out that $\tan(\theta)$ is equal to $\tan(\theta + \pi)$ such that there are two inverses for any given angle θ . Moreover, the trigonometric function \tan^{-1} ('arctan') has a range of $(-\frac{\pi}{2}, \frac{\pi}{2})$. The definition of the circular mean direction $\bar{\theta}$

given in Equation (1) takes the signs of C and S into account and provides a unique inverse on the interval $[0, 2\pi)$.

Note that there exists no circular mean direction, if the length of the resultant vector is equal to zero, implying that the data observed are not concentrated towards any preferred direction (Jammalamadaka and SenGupta, 2001, p. 15).

5.2.4 Circular Median Direction

Another measure of location for circular data is the *sample median direction* $\tilde{\theta}$. It can be determined similarly to the median for linear data. Hence, $\tilde{\theta}$ is any angle ϕ such that half of the data points lie in the arc $[\phi, \phi + \pi)$ and the majority of the data points are nearer to ϕ than to $\phi + \pi$ (Mardia and Jupp, 2000, p. 17). If the sample size n is odd, the median is the one of the data points, and if the number of data points n is even, the median direction passes through the midpoint of two adjacent data points (Mardia and Jupp, 2000, p. 17). Fisher (1993, p. 35) points out that the median direction is only unique for reasonably unimodal data, but may not be uniquely defined with multimodal or isotropic data.

5.2.5 Sample Circular Variance

A frequently used measure of dispersion of angular data is the *sample circular variance* V , which is defined by

$$V = 1 - \bar{R} ,$$

where V can take values in the range of $[0, 1]$ (Fisher, 1993, p. 32). Its interpretation is similar to the variance of linear data, i.e. “the smaller the value of the circular variance, the more concentrated the distribution” (Fisher, 1993, p. 32).

5.2.6 Circular Standard Deviation

Always closely related to the variance is the standard deviation. When dealing with circular data, it is called *circular standard deviation* v and is calculated via the following equation

$$v = \{-2 \log(1 - V)\}^{1/2} = \{-2 \log \bar{R}\}^{1/2} ,$$

which reduces to

$$v \simeq (2V)^{1/2} = \{2(1 - \bar{R})\}^{1/2} ,$$

if the sample circular variance V is small (Mardia and Jupp, 2000, p. 19). Other than V , v has a range of $[0, \infty)$ (Mardia and Jupp, 2000, p. 19).

5.2.7 Circular Range

Another measure of dispersion is the *circular range* w , which is defined as “the length of the smallest arc which contains all the observations” (Mardia and Jupp, 2000, p. 20). In order to calculate it, the circle is cut at the initial direction and the linear order statistics of θ_i , $1 \leq i \leq n$, are determined, which are denoted by $\theta_{(1)} \leq \dots \leq \theta_{(n)}$. These are used to compute the arc lengths between two adjacent observations by

$$T_i = \theta_{(i+1)} - \theta_{(i)} , \quad i = 1, \dots, n-1 ; \quad T_n = 2\pi - \theta_{(n)} + \theta_{(1)} .$$

Eventually, the circular range w is given by

$$w = 2\pi - \max(T_1, \dots, T_n)$$

(Mardia and Jupp, 2000, p. 20).

The order statistics of the three directions in the example given at the beginning of Subsection 5.2 are $\theta_{(1)} = 0^\circ$, $\theta_{(2)} = 45^\circ$ and $\theta_{(3)} = 315^\circ$. Thus, the circular range is $w = 360^\circ - \max(45^\circ, 270^\circ, 45^\circ) = 90^\circ$.

6 Statistical Analysis

The statistical methods for circular data presented above are now applied to the data described in Section 4. First, the data sets of each specimen will be examined individually in terms of the orientations of the cracks. Afterwards, both assays will be compared with a particular regard to the question, whether the behavior of the cracks differs. The whole analysis is conducted using the statistical software R (R Development Core Team, 2009).

6.1 Computation of the Angles

The data sets of both specimens only contain the lengths of the cracks paths, the sizes of the crack clusters and the x - and y -coordinates of the start and end points of the crack paths. The orientations of the cracks, however, are not listed and need to be calculated before the analysis can begin. In order to determine the angles, the differences of the start

and end points of each micro crack are computed, i.e. ‘End_x – Begin_x’ and ‘End_y – Begin_y’. Denote the former difference by `diff.x` and the latter one by `diff.y`, then an angle can be calculated by applying Pythagoras’ Theorem

$$\cos(\theta) = \frac{\text{adjacent}}{\text{hypotenuse}} = \frac{\text{diff.x}}{\sqrt{\text{diff.x}^2 + \text{diff.y}^2}}.$$

Next, the inverse trigonometric function \cos^{-1} (‘arccosine’) needs to be used on both sides of the equation. Since the domain of \cos^{-1} is $[0, \pi]$, all resulting angles take values between 0° and 180° .

Note that the start and end points were chosen arbitrarily and that the stress is given in vertical direction, i.e. the 90° angle.

6.2 Crack Analysis of Specimen 10

In order to gain a first idea of the cracks observed in Specimen 10, the number of all cracks per time point are determined, which can be found in Table 1.

Table 1: Number of all cracks per load cycles

Specimen 10					
load cycles	all cracks	load cycles	all cracks	load cycles	all cracks
0	432	10000	3798	20000	6284
1000	508	11000	4394	25000	5997
2000	582	12000	4592	30000	6215
3000	1328	13000	4798	35000	9456
4000	1785	14000	3696	37000	8178
5000	2210	15000	4988	39000	8356
6000	2598	16000	5130	40000	8184
7000	3058	17000	5214	42000	4940
8000	3070	18000	5810	44000	7217
9000	3472	19000	6066		

The main thing to notice is that overall the number of cracks increases. Particularly, towards the end of the experiment, i.e. past 35000 load cycles, much more cracks are present. This is attributed to the fact that the material fatigues the more load cycles are applied and hence more cracks are generated. However, at some points of time there are actually less cracks than the immediate prior time point, e.g. after 14000 and 42000 load

cycles. One possible explanation for this phenomenon is that micro cracks gradually grow and eventually merge with other micro cracks to form macro cracks, which in turn reduces the number of cracks. Another explanation is that the poor quality and light exposure of some images sometimes complicates the detection of all cracks.

Surprisingly, the recognition program detects 432 cracks even before the fatigue loading has begun. In Table 2 the cracks are divided into groups of different lengths and the corresponding frequencies are listed. The table shows that cracks up to a length of 25 μm make up the most part of the total number of cracks.

Table 2: Number of cracks per load cycles, grouped by different lengths

Specimen 10									
load					load				
cycles	0-10	10-30	30-70	≥ 70	cycles	0-10	10-30	30-70	≥ 70
0	395	34	2	1	15000	4673	309	6	1
1000	467	35	4	3	16000	4820	302	11	1
2000	545	33	4	1	17000	4876	327	10	1
3000	1268	55	4	1	18000	5423	371	16	1
4000	1710	70	4	1	19000	5637	415	16	1
5000	2117	88	4	1	20000	5845	422	17	1
6000	2482	112	4	1	25000	5564	415	18	1
7000	2921	132	5	1	30000	5722	470	23	1
8000	2921	143	5	1	35000	8570	812	71	3
9000	3286	181	4	1	37000	7455	672	50	2
10000	3604	186	7	1	39000	7586	707	60	3
11000	4145	242	7	1	40000	7459	665	56	6
12000	4316	271	6	1	42000	4591	326	21	3
13000	4500	288	9	1	44000	6635	530	45	7
14000	3503	189	3	1					

Müller et al. (2011) comment that the majority of those short cracks are caused by surface roughness, pits and scratches and are therefore no real cracks. To increase the chance of dealing just with the ‘real’ ones, all cracks shorter than 10 pixels will be excluded from the analysis. This procedure reduces the number of cracks drastically, see Table 15 in Appendix A.2. At time point 0, for instance, only 37 cracks are longer than 10 pixels. Their orientations are visualized in Figure 10.

On the left hand side the frequencies are displayed in a linear histogram with 10°-intervals and on the right hand side they are visualized via a circular raw data plot. Both

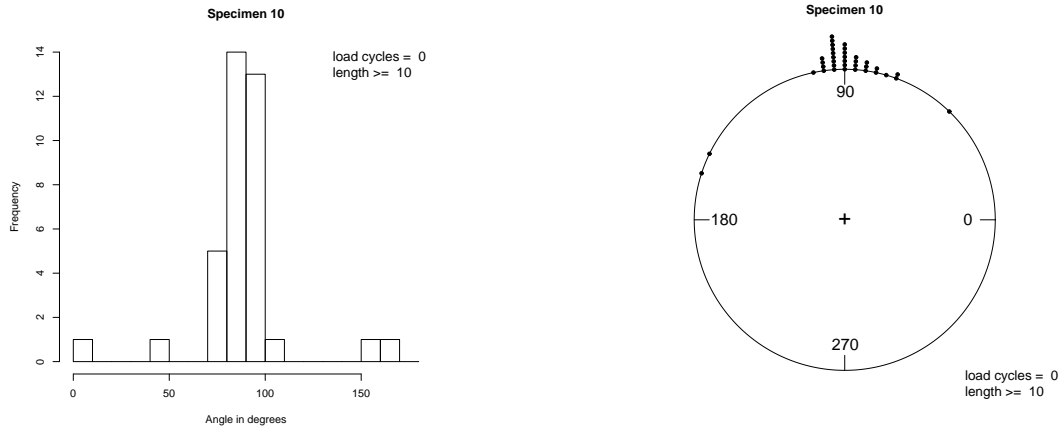


Figure 10: Crack orientations before experiment started

plots indicate that the cracks prefer an orientation in direction of 90° . More precisely, 6 of the 37 cracks have an orientation of exactly 90° . These, however, are more likely to be scratches that were generated while polishing the specimen. It also stands out that the orientations are almost symmetrically distributed around the 90° angle. This symmetry led to another idea: reflecting the angles along the vertical direction. Remember that all angles range between 0° and 180° . Since it is only of interest how the cracks orient with respect to the loading axis, but not whether they propagate to the left or to the right, it is sufficient to focus on the interval $[0^\circ, 90^\circ]$. To include all cracks, angles between 90° and 180° are reflected along the 90° angle. This procedure simplifies the interpretation of the crack orientations, in particular, if those are represented in a rose diagram, e.g. see Figure 11. This plot contains the same angles as in Figure 10 and it emphasizes what has been concluded before: most cracks have an angle close to 90° .

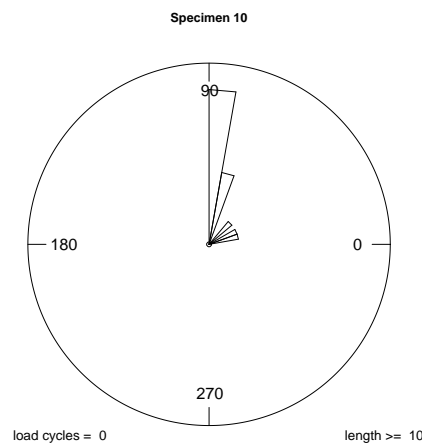


Figure 11: Rose diagram of crack orientations before fatigue loading started

Next, the maximum lengths of the cracks per number of load cycles are identified and listed in Table 3.

Table 3: Maximum length of the cracks per load cycles (in pixels)

Specimen 10					
load	max.	load	max.	load	max.
cycles	length	cycles	length	cycles	length
0	72.57	10000	84.01	20000	84.43
1000	73.83	11000	85.43	25000	84.84
2000	74.25	12000	87.25	30000	88.70
3000	84.84	13000	88.43	35000	118.08
4000	86.08	14000	85.43	37000	114.84
5000	86.25	15000	84.84	39000	126.01
6000	86.67	16000	84.50	40000	149.23
7000	86.25	17000	83.84	42000	113.60
8000	84.84	18000	86.25	44000	325.84
9000	87.25	19000	86.25		

As expected, the maximum length increases steadily over time. Especially, at the end, namely after 35000 load cycles, it advances rather quickly. This again can be traced back to the fact that micro cracks propagate and merge with one another, i.e. the cracks become longer. However, if the longest crack is omitted at each time point, the maximum length clearly changes, e.g. it drops from 72.57 pixels to 32.90 pixels at time point 0 (see Table 16, Appendix A.2). This phenomenon can easily be explained, when taking Table 2 into account once more. Apparently, only few cracks have a length greater than 30 pixels. Moreover, up to 35000 load cycles there is only one crack per time point that is longer than 70 pixels. The only exception is time point 1000 with 3 long cracks.

6.2.1 Orientation at Initial Stage

Since the majority of the cracks is not longer than 30 pixels (see Table 2), long cracks will be excluded from the following analysis. Consequently, only cracks with a minimum length of 10 pixels and a maximum length of 30 pixels will be taken into account for the analysis of the crack orientations at the early phase of the standard fatigue experiment.

In order to find out whether the cracks have an orientation of about 45° at the initial stage of crack propagation, the mean direction is calculated. Note that because of the

reflection along the 90° angle, an orientation of 45° includes angles of 135° as well. The circular mean direction, the mean resultant length and the circular variance of the first seven time points, i.e. up to and including 7000 load cycles, are given in Table 4. A complete list of the measures of location and dispersion for all time points can be found in Table 17 in Appendix A.2.

Table 4: Measures of location and dispersion at initial stage ($10 \leq \text{length} \leq 30$)

Specimen 10							
	load cycles						
	1000	2000	3000	4000	5000	6000	7000
number of cracks	35	33	55	70	88	112	132
circular mean direction	81.56°	77.93°	69.97°	62.33°	49.94°	44.86°	41.23°
mean resultant length	0.98	0.95	0.91	0.86	0.84	0.85	0.86
circular variance	0.02	0.05	0.09	0.14	0.16	0.15	0.14

The figures in Table 4 clearly show that the mean direction decreases the more stress is applied to the material. Moreover, the assumption that initial cracks have an average orientation of approximately 45° seems to be verified, especially after 6000 but even after 7000 load cycles. The mean resultant lengths are close to 1, meaning that the angles are quite coincident. The low variances indicate the same. The rose diagrams of these two specific time points illustrate the distribution of the angles, see Figure 12. Rose diagrams of the crack orientations after 1000, 2000, 3000, 4000 and 5000 load cycles can be found in Appendix A.1, Figures 24, 25 and 26.

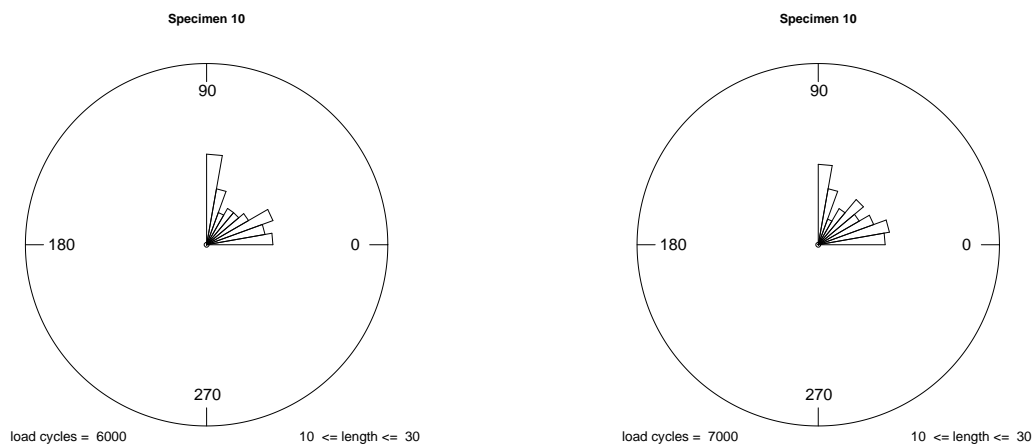


Figure 12: Orientations of the cracks after 6000 load cycles (left) and 7000 load cycles (right)

The plots do not allow a definite identification of a preferred direction. Nonetheless, the measures and rose diagrams suggest that progressive strain causes the orientations of the micro cracks to change. Less cracks have an angle close to 90° and the average direction diminishes. In other words, the cracks tend gradually more towards the 0° angle as successively more load cycles are applied. Moreover, the cracks in Specimen 10 approach a mean orientation of 45° after about 6000 load cycles, if cracks with a length between 10 and 30 pixels are considered. This is even true, if cracks up to 70 pixels are included, see Table 19, Appendix A.2. Also, including all cracks longer than 10 pixels has only little effect on the mean direction (Table 5).

To complete the analysis of the crack orientations at the initial stage, the circular mean directions of cracks shorter than 10 pixels, longer than 30 pixels and cracks of all lengths are each listed in Table 5. The missing time points 8000 to 44000 are given in Appendix A.2, Table 18.

Table 5: Circular mean directions at initial stage, grouped by different lengths

Specimen 10							
	<u>load cycles</u>						
	1000	2000	3000	4000	5000	6000	7000
$0 \leq \text{length} \leq 10$	48.73°	38.10°	28.65°	25.84°	23.98°	23.96°	22.48°
$\text{length} \geq 10$	83.83°	75.10°	69.68°	62.51°	50.56°	45.57°	42.42°
$\text{length} \geq 30$	71.83°	54.39°	66.26°	64.96°	61.52°	61.99°	69.38°
all cracks	51.65°	40.79°	30.49°	27.30°	25.04°	24.86°	23.35°

Again, the circular mean direction decreases over time. Apparently, it was a good choice of filtering out short cracks, since their mean directions are small and they influence the mean direction of all cracks immensely. Since most of them are scratches and impurities, they would have falsified the results.

6.2.2 Orientation at Stable Propagation Stage

To investigate whether the orientation of the cracks is perpendicular to the stress towards the end of the fatigue process, measures of location and dispersion for all time points are determined and can be found in Appendix A.2 in Table 19. This time, cracks with a length of up to 70 pixels are included such that longer cracks, which develop during the experiment, are considered as well. The table shows that the circular mean direction

and the circular median direction decrease over time. Especially, during the early phase both measures of location diminish very fast. After about 12000 load cycles, however, they level out. While the mean direction mainly fluctuates between 27° and 31° , the median direction ranges from 20° to 24° with an exception of 26.57° at time point 14000.

Of high interest is now the last time point, i.e. after 44000 load cycles have been applied. A rose diagram of the cracks' angles is given on the left hand side of Figure 13.

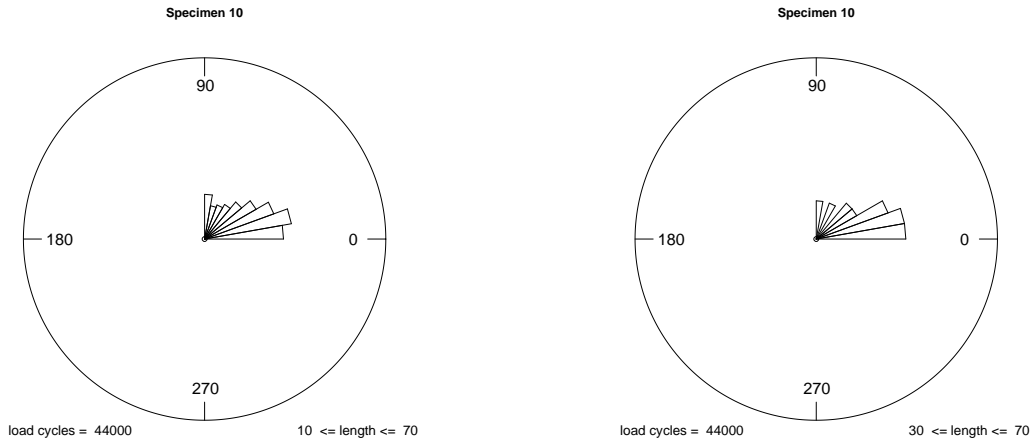


Figure 13: Orientations of the cracks after 44000 load cycles. Left: $10 \leq \text{length} \leq 70$; Right: $30 \leq \text{length} \leq 70$

Since 575 cracks with a length between 10 and 70 pixels were detected at the end of the experiment, the minimum length of the crack path is raised to 30 pixels. Thus, the focus is set only on the longest cracks present. Left are 45 cracks, which illustrate even better that macro cracks trend to have a horizontal orientation with respect to the loading axis, see right hand side of Figure 13.



Figure 14: Orientations of the cracks after 44000 load cycles. Left: $\text{length} \geq 40$; Right: $\text{length} \geq 70$

Moreover, if all cracks longer than 40 pixels, i.e. the 24 longest macro cracks, or all cracks longer than 70 pixels, i.e. the 7 longest macro cracks, are considered, the assumption of a perpendicular orientation is further substantiated, see Figure 14.

Table 6: Mean direction after 44000 load cycles

Specimen 10		
	number of cracks	circular mean direction
$10 \leq \text{length} \leq 30$	530	28.80°
$10 \leq \text{length} \leq 70$	575	28.14°
$30 \leq \text{length} \leq 70$	45	20.58°
$\text{length} \geq 40$	24	12.68°
$\text{length} \geq 70$	7	6.84°

Table 6 contains the mean directions of all cases just mentioned. Note that the average direction decreases the more cracks of shorter length are filtered out. This inference reinforces the hypothesis of long cracks preferring a perpendicular orientation.

6.3 Crack Analysis of Specimen 31

The investigation of Specimen 31 starts off with determining the number of all cracks present per load cycle. They are listed in Table 7. Once again, it can be seen that more cracks appear the longer the fatigue loading lasts. Apparently, this specimen contains much more cracks than Specimen 10, which is due to the higher stress level applied.

Table 7: Number of all cracks per load cycle

Specimen 31			
load	all	load	all
cycles	cracks	cycles	cracks
0	388	8000	7957
1000	426	9000	8213
2000	981	10000	9019
3000	1650	12000	9892
4000	2990	14000	11510
5000	4842	16000	11325
6000	5137	18000	12449
7000	6842		

An interesting observation is made when identifying the maximum crack length per load cycle, see Table 8. The maximum length varies a lot in this assay and grows much faster than it did in Specimen 10. Especially, after the first 1000 load cycles and between 5000 and 6000 load cycles, the maximum length decreases considerably from 113.43 pixels to 66.94 pixels and from 94.25 pixels to 59.28 pixels, respectively.

Table 8: Maximum length of cracks per load cycle

Specimen 31			
load	max.	load	max.
cycles	length	cycles	length
0	113.43	8000	91.98
1000	66.94	9000	94.76
2000	91.77	10000	97.30
3000	92.15	12000	81.50
4000	102.91	14000	121.71
5000	94.25	16000	137.30
6000	59.28	18000	262.55
7000	93.50		

This oddity can be explained by looking at the total image of Specimen 31 at the beginning of experiment, which clearly shows a big crater in the upper middle part (see left hand side of Figure 3). This crater is accountable for the longest crack at the beginning, but its influence vanishes as the experiment progresses. Nevertheless, this has to be paid attention to in the analysis of the data. Naturally, it would be best to eliminate craters and big scratches from the data sets, but since a definite identification of the cracks is rather complicated, this idea has to be put aside for now.

However, it is possible to determine the longest cracks per time point. A table of the maximum lengths after the longest crack is excluded is given in Table 20, Appendix A.2, and it shows once more how this course of action effects the maximum lengths. For instance, it decreases from 91.77 pixels to 39.97 pixels at time point 2000. All these aspects led once more to the decision to divide the cracks into groups of different lengths and to determine the corresponding frequencies, which are displayed in Table 9.

As seen before with Specimen 10, the majority of the cracks have a length between 0 and 10 pixels. Since it is assumed that those are mainly scratches and impurities, they are once again excluded from the analysis in order to avoid a falsified result.

Table 9: Number of cracks per load cycles, grouped by different lengths

Specimen 31				
load cycles	0-10	10-30	30-70	≥ 70
0	359	30	1	1
1000	402	21	3	0
2000	943	37	1	1
3000	1544	103	3	1
4000	2798	185	6	1
5000	4475	351	16	1
6000	4742	373	23	0
7000	6247	555	40	1
8000	7180	715	64	1
9000	7401	746	63	3
10000	8068	866	83	3
12000	8761	999	134	2
14000	9992	1315	194	10
16000	9839	1274	197	18
18000	10799	1363	254	33

6.3.1 Orientation at Initial Stage

The preferred direction of the micro cracks at the beginning of the fatigue loading is examined by calculating the measures of the crack orientations. As with Specimen 10, first, only cracks longer than 10 pixels and shorter than 30 pixels are considered. A complete list of all time points is given in Table 21 in Appendix A.2.

Table 10: Measures of location and dispersion ($10 \leq \text{length} \leq 30$)

Specimen 31					
	load cycles				
	0	1000	2000	3000	4000
number of cracks	30	21	37	103	185
circular mean direction	82.75°	77.77°	52.70°	39.38°	30.55°
mean resultant length	0.97	0.96	0.84	0.88	0.91
circular variance	0.03	0.04	0.16	0.12	0.09

The main point to notice in Table 10 is that the circular mean direction decreases much faster than it did in Specimen 10. A mean angle of 45° is passed by after time point

3000. For rose diagrams of the cracks' angles after 2000 and 3000 load cycles see Figure 15. Time points 1000 and 4000 are given in Appendix A.1, Figure 27.

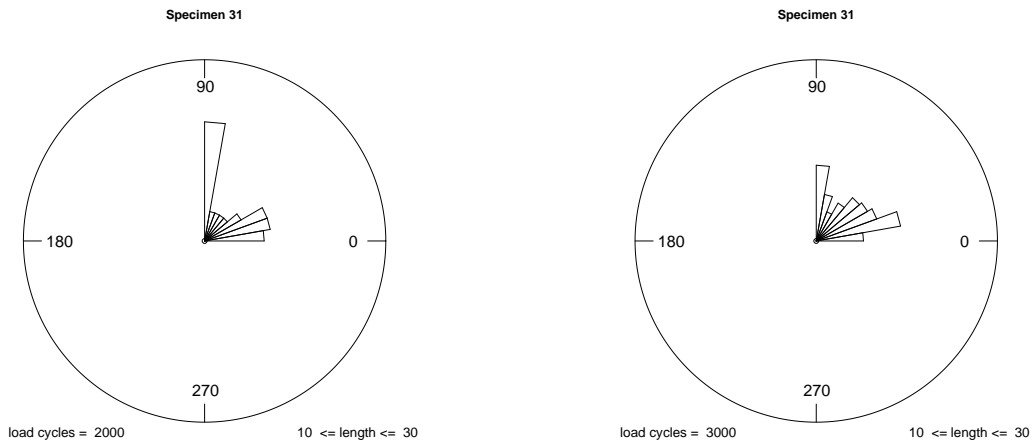


Figure 15: Orientations of the cracks. Left: after 2000 load cycles; Right: after 3000 load cycles

Although there are not many cracks longer than 30 pixels present during the early phase, it is checked, whether an inclusion of them has an effect on the result. The figures in Table 11 show that this is not the case. Moreover, the table lists the mean directions of cracks shorter than 10 pixels, longer than 30 pixels and cracks of all lengths. The missing time points 5000 to 18000 can be found in Appendix A.2, Table 22.

Table 11: Circular mean directions at initial stage, grouped by different lengths

Specimen 31					
	load cycles				
	0	1000	2000	3000	4000
$0 \leq \text{length} \leq 10$	51.32°	40.32°	27.75°	22.81°	21.23°
$\text{length} \geq 10$	80.65°	75.16°	51.81°	39.34°	30.55°
$\text{length} \geq 30$	48.07°	55.10°	36.16°	38.31°	30.42°
all cracks	53.79°	42.53°	28.72°	23.84°	21.84°

Table 11 clarifies that cracks shorter than 10 pixels have a big influence on the mean direction. Therefore, filtering them out was once again a good decision. However, it is to keep in mind that it is not known how many of them might actually be 'real' cracks and hence should be included. Thus, an identification of the cracks would be very useful.

All in all, when looking at the rose diagrams and the measures, it is apparent that a higher stress level causes cracks to grow faster, thus changing their orientations faster as

well. An average direction of 45° is passed by after only applying 3000 load cycles, while Specimen 10 had to be exposed to more than 6000 load cycles to get the same result.

6.3.2 Orientation at Stable Propagation Stage

Towards the end of the experiment, Specimen 31 behaves similarly to Specimen 10, that is the angles become successively smaller. In other words the cracks orient gradually more horizontal with respect to the stress. Since the micro cracks grow as the experiment progresses (see Table 9), these evolving macro cracks become more important towards the end. Therefore, cracks up to a length of 70 pixels are included in the following analysis.

A complete list of the measures of location and dispersion of angles with a length between 10 and 70 pixels can be found in Appendix A.2, Table 23. As expected, the circular mean direction and the circular median direction become smaller just like they did in Specimen 10. However, it happens much faster in this case. Moreover, both measures level out rather soon. After 4000 load cycles up until the end, they fluctuate between 28° and 32° and between 23° and 27° , respectively. The mean resultant length has a constant value of 0.93 and the variance is very low with values around 0.07. This indicates a tightly clustered distribution of the observations. The orientations after 10000 and 18000 load cycles are visualized in Figure 16.

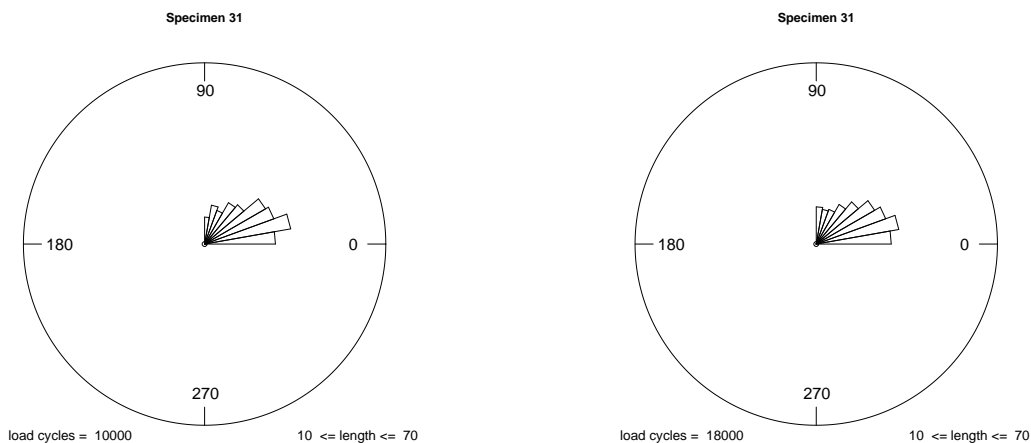


Figure 16: Orientations of the cracks. Left: after 10000 load cycles; Right: after 18000 load cycles

When raising the minimum length to 40 pixels or even 70 pixels, the tendency towards a perpendicular orientation becomes more evident. For one, the number of cracks decreases noticeably, and furthermore, the mean direction decreases to 25.03° and 19.06° ,

respectively, see Table 12.

Table 12: Mean direction after 18000 load cycles

Specimen 31		
	number of cracks	circular mean direction
$10 \leq \text{length} \leq 30$	1363	29.48°
$10 \leq \text{length} \leq 70$	1617	29.37°
$30 \leq \text{length} \leq 70$	254	28.77°
$\text{length} \geq 40$	157	25.03°
$\text{length} \geq 70$	33	19.06°

This is well illustrated in both rose diagrams in Figure 17, especially when comparing them with the ones in Figure 16.

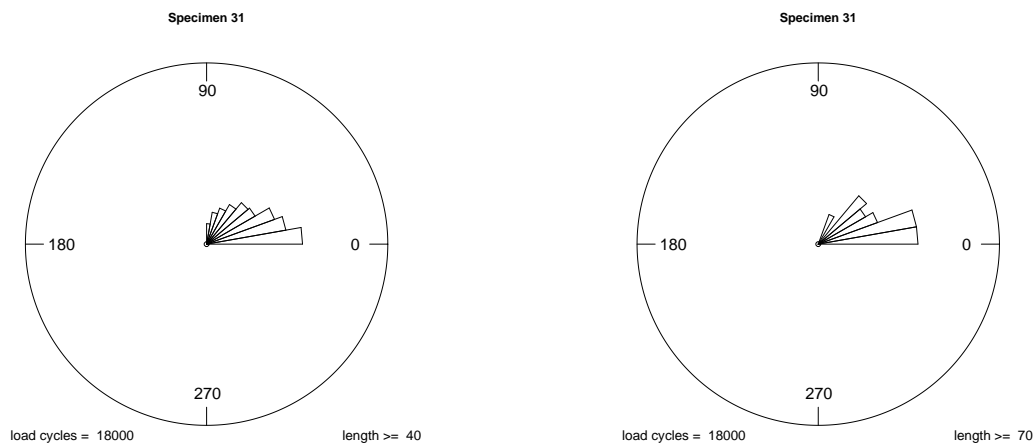


Figure 17: Orientations of the cracks after 18000 load cycles. Left: $\text{length} \geq 40$; Right: $\text{length} \geq 70$

In summary, a perpendicular orientation of the angles after the experiment ended can not be disclaimed, although it is not as distinctive as it is after 44000 load cycles in Specimen 10.

6.4 Comparison between Specimen 10 and Specimen 31

Remember that Specimen 10 and Specimen 31 were exposed to different stress levels. A stress level of 360 MPa was applied to Specimen 10, while Specimen 31 obtained 400 MPa. It makes sense that a higher stress level results in a faster damage evolution. In this case it means that the material fatigues sooner due to a quicker growth of the cracks and a

higher number of cracks, see Figure 18. Note that the fluctuation of the number of cracks present in Specimen 10, in particular towards the end, might also be due to the different qualities and light exposures of the image segments examined.

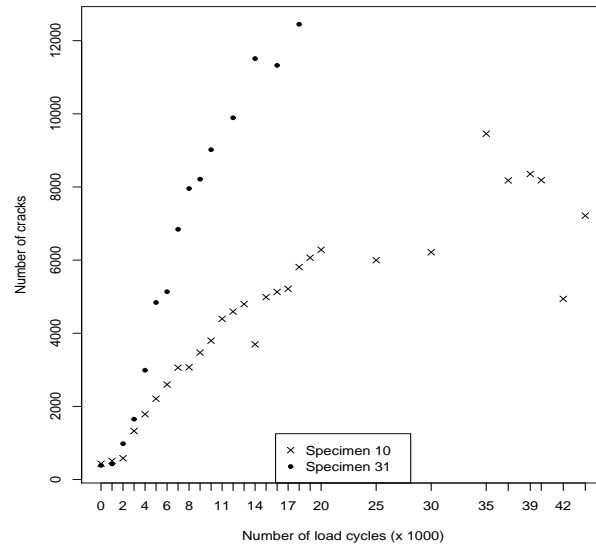


Figure 18: Number of all cracks of both specimens

Because of the analysis conducted in the former two subsections, it is already known that the orientations of the cracks change the more load cycles are applied. This is true for either specimen. Of interest is now, whether the stress level influences this behavior by causing a quicker change of the orientations of the micro cracks. To allow a fair analysis of the two assays, only cracks with a minimum length of 10 pixels and a maximum length of 70 pixels are considered. First, both specimens are compared by looking at rose diagrams.

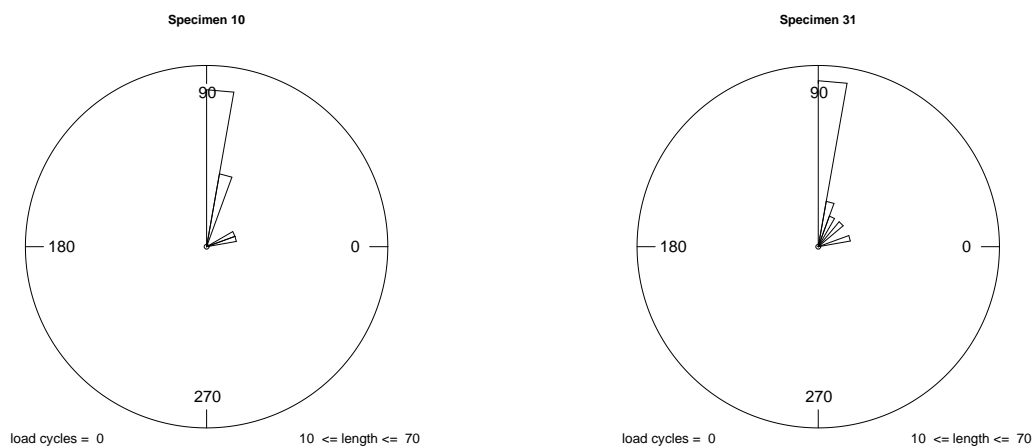


Figure 19: 0 load cycles. Left: Specimen 10; Right: Specimen 31

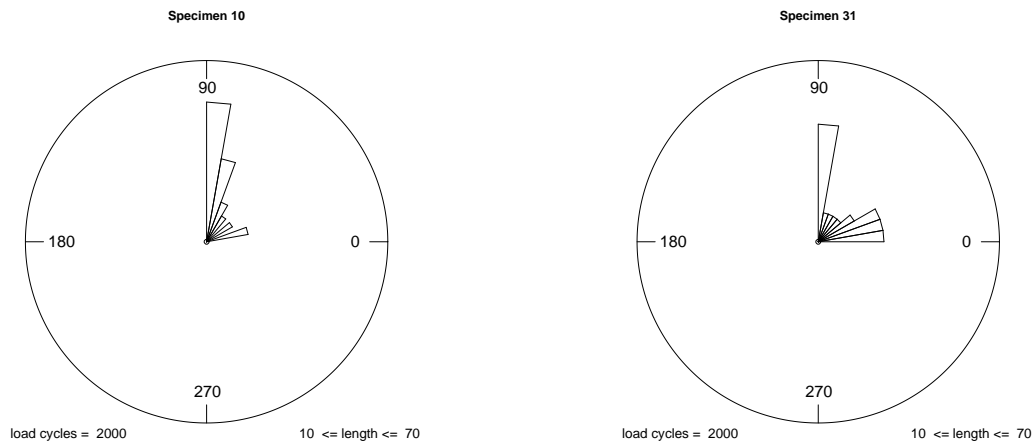


Figure 20: 2000 load cycles. Left: Specimen 10; Right: Specimen 31

While the orientations behave similarly at the beginning of the experiment (Figure 19), a slight difference is noticeable at time point 2000, see Figure 20. Time point 1000 is given in Appendix A.1, Figures 28. After 2000 load cycles, a lot of cracks in Specimen 31 already propagate with an angle between 0° and 30° , whereas the majority of the cracks in Specimen 10 still have a preferred direction of 80° to 90° . This behavior slowly changes as the experiment continues (Figures 29 and 30 in Appendix A.1), but an apparent difference still exists after 5000 load cycles, see Figure 21.

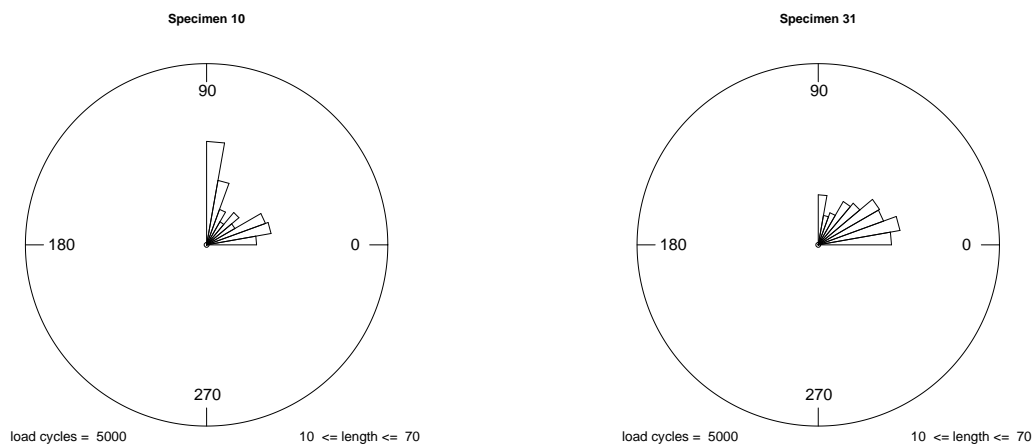


Figure 21: 5000 load cycles. Left: Specimen 10; Right: Specimen 31

It is not until after 10000 load cycles that the cracks act similarly again (Appendix A.1, Figure 31). After 18000 load cycles, see Figure 22, the orientations seem to be very much alike. All rose diagrams support the idea that the angles of a specimen exposed to a higher stress level decrease faster, i.e. the cracks start to orient perpendicular to the loading axis sooner.

This conclusion can be checked with the distribution-free Wilcoxon test. Its big ad-

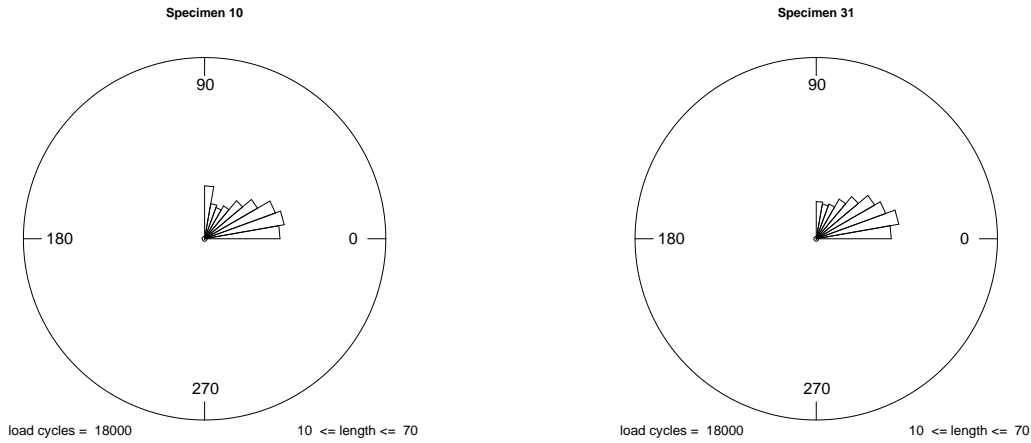


Figure 22: 18000 load cycles. Left: Specimen 10; Right: Specimen 31

vantage is that it is only based on the ranks of the observations such that outliers have no influence. In this case, it is used for testing whether the circular mean direction behaves differently in both specimens. Additionally, 95% Wilcoxon confidence intervals are calculated. The null hypothesis and alternative hypothesis for the Wilcoxon test conducted are formulated as follows:

H_0 : “The orientations of the cracks do not differ in both specimens.”

H_1 : “The orientations of the cracks differ in both specimens.”

If the p-value, i.e. the probability under the null hypothesis to obtain a more extreme value of the test statistic, is smaller than a given significance level, H_0 is rejected. Here, a significance level of 5% is chosen.

Since there only exist data up to 18000 load cycles for Specimen 31, it makes sense to compare the two specimens only up to that time point. Figure 23 shows the circular mean directions of each specimen for all time points and the corresponding 95% Wilcoxon confidence intervals. The plot illustrates very well how the orientations of the cracks differ, particularly, between time points 2000 and 8000. However, at the beginning, after 1000 load cycles and after 12000 load cycles up until the end, the confidence intervals overlap, which indicates that there is not a statistically significant difference between the two specimens for the circular mean directions at those time points.

This needs to be checked by applying the two-sample Wilcoxon test. The resulting p-values are given in Table 13. The table shows that the null hypothesis can be rejected after 2000 load cycles up to and including 8000 load cycles and once again after 10000 load cycles. Hence, the orientations of the cracks in Specimen 10 and Specimen 31 significantly

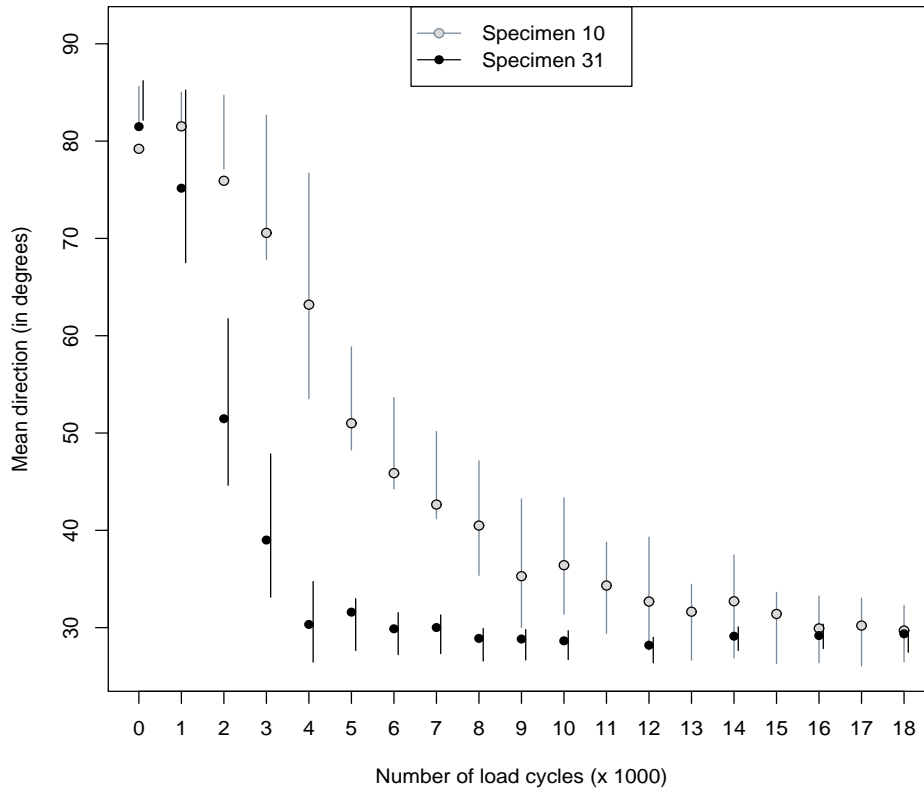


Figure 23: Circular mean directions and 95% Wilcoxon confidence intervals for each specimen ($10 \text{ pixels} \leq \text{crack length} \leq 70 \text{ pixels}$)

differ at these points of time. Before and after, H_0 can not be rejected.

Table 13: P-values of the two-sample Wilcoxon test

load cycles	0	1000	2000	3000	4000	5000	6000	7000
p-value	0.4799	0.5459	0.0098	0.0000	0.0000	0.0000	0.0000	0.0002
load cycles	8000	9000	10000	12000	14000	16000	18000	
p-value	0.0002	0.0754	0.0030	0.3143	0.3036	0.8134	0.6230	

It can be concluded that both specimens provide the same starting and ending conditions. Furthermore, an early distinction between an assay exposed to a lower stress level and an assay exposed to a higher stress level seems to be possible.

7 Conclusion

A standard fatigue experiment was performed, where two specimens of low carbon steel, namely Specimen 10 and Specimen 31, were exposed to different stress levels. While the former one obtained a level of 360 MPa, a higher level of 400 MPa was applied to the latter one. After predefined time points, given as the number of load cycles, the surfaces were scanned via a long-distance microscope and hundreds of images were taken with a 1.14 MPig b/w camera. These images built the foundation of the analysis conducted in this paper.

Applying the R package `crackrec` to the images of each specimen provided two data sets that contain the information of all cracks present in each specimen for all predefined points of time. The variables included `length` (lengths of the cracks paths), `size` (sizes of the crack clusters), `Begin_x`, `Begin_y`, `End_x` and `End_y` (x - and y -coordinates of the start and end points of the crack paths). Of interest were the crack orientations during the initial stage and the stable propagation stage of the fatigue process. In addition, it was examined how the behavior of the cracks resembles or differs when comparing Specimen 10 with Specimen 31. Since the focus was set on the orientation of the cracks, circular statistics instead of linear statistics had to be applied.

The first hypothesis to be investigated was whether the micro cracks have an orientation of approximately 45° with respect to the loading axis in the early phase of the damage evolution. This assumption could be reinforced for either specimen. While it took about 6000 load cycles for Specimen 10, only about 3000 load cycles had to be applied to Specimen 31, which obtained a higher stress level. The circular mean directions for cracks with a length between 10 and 30 pixels at those time points were 44.86° and 39.38° , respectively.

The second hypothesis was that cracks tend to have an orientation perpendicular to the stress towards the end of the experiment and after micro cracks have become macro cracks. After the fatigue process was finished, the circular mean direction of cracks longer than 70 pixels turned out to be 6.84° and 19.06° for Specimen 10 and Specimen 31, respectively. Therefore, this assumption could be substantiated as well.

Last but not least, both specimens were compared with one another. With the help of the two-sample Wilcoxon test it could be concluded that the crack orientations statistically significant differ during the intermediate stage of crack propagation. i.e. after 2000 load

cycles up to and including 10000 load cycles, with one exception of time point 9000. Thus, the circular mean direction is able to discriminate between two assays that were exposed to different stress levels at an early stage of the standard fatigue experiment. It follows that the circular mean direction is a more useful parameter than the parameters examined by Müller et al. (2011) such as the number of crack clusters or the cumulative length, because those can only be determined by taking all image segments into account. As for the circular mean direction, one image segment is sufficient.

It is to keep in mind that the image segments investigated in this paper are blurred and contain shadows, which affects the quality of the pictures and complicates a proper crack detection. Additionally, the scratches, pits and other impurities make an identification of ‘real’ cracks very difficult. Hence, it would be helpful to identify all cracks individually in order to find out which are real cracks and which are not. Then, the latter ones could be filtered out such that only real micro cracks are considered in the analysis.

A possible solution of finding and eliminating scratches or craters in a data set, is to relate the length of a crack path to the size of the corresponding crack cluster. Describing the crater as a circle, where r denotes its radius, its diameter could be defined by the variable `length`, i.e. $2 \cdot r$ and `size` can be regarded as the circle’s area, i.e. $\pi \cdot r^2$. In order to get rid of the variable r , `length` has to be squared:

$$\frac{\text{length}^2}{\text{size}} = \frac{4 \cdot r^2}{\pi \cdot r^2} = \frac{4}{\pi} \approx 1.2732 .$$

Hence, applying a constraint such as $\frac{\text{length}^2}{\text{size}} > 3$ to the data sets should eliminate craters. It might be reasonable to choose a larger value on the right hand side of this inequality, if it is apparent that big craters are present such as the big crater in the upper middle part in the composed total image of Specimen 31.

In future studies it should be examined whether this constraint is really applicable and helpful. If this is the case, it needs to be investigated what values should be used. Moreover, developing a constraint for eliminating scratches would be very valuable, since those make up most of the short cracks. One idea is to omit cracks with an angle of exactly 90° at the beginning of the experiment, because most of them are scratches that were caused by polishing the specimens. However, some of them might actually be real cracks. Thus, it would be of great help to develop an improved way of distinguishing between ‘real’ cracks and ‘non-real’ cracks.

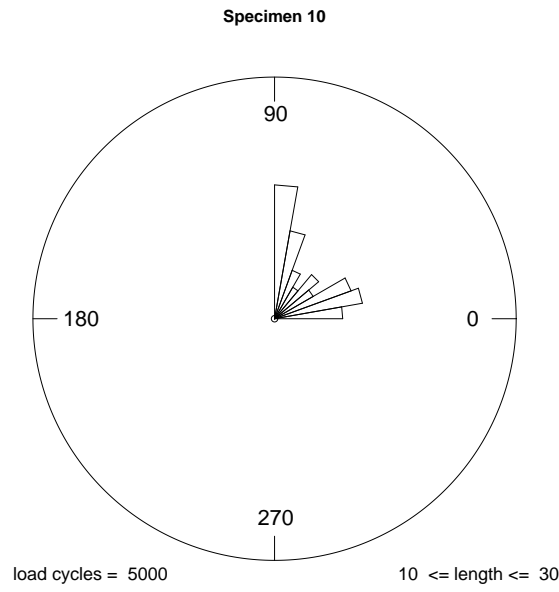


Figure 26: Crack orientations after 5000 load cycles

Section 6.3.1: Crack orientations of Specimen 31 at Initial Stage

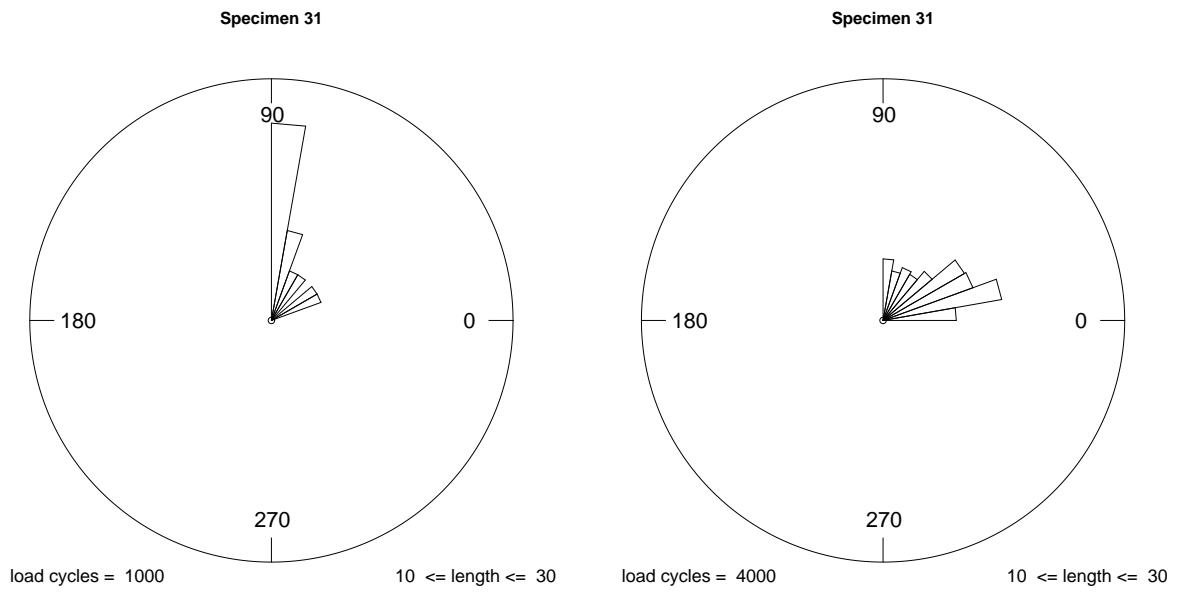


Figure 27: Crack orientations after 1000 load cycles (left) and 4000 load cycles (right)

Section 6.4: Comparison between Specimen 10 and Specimen 31

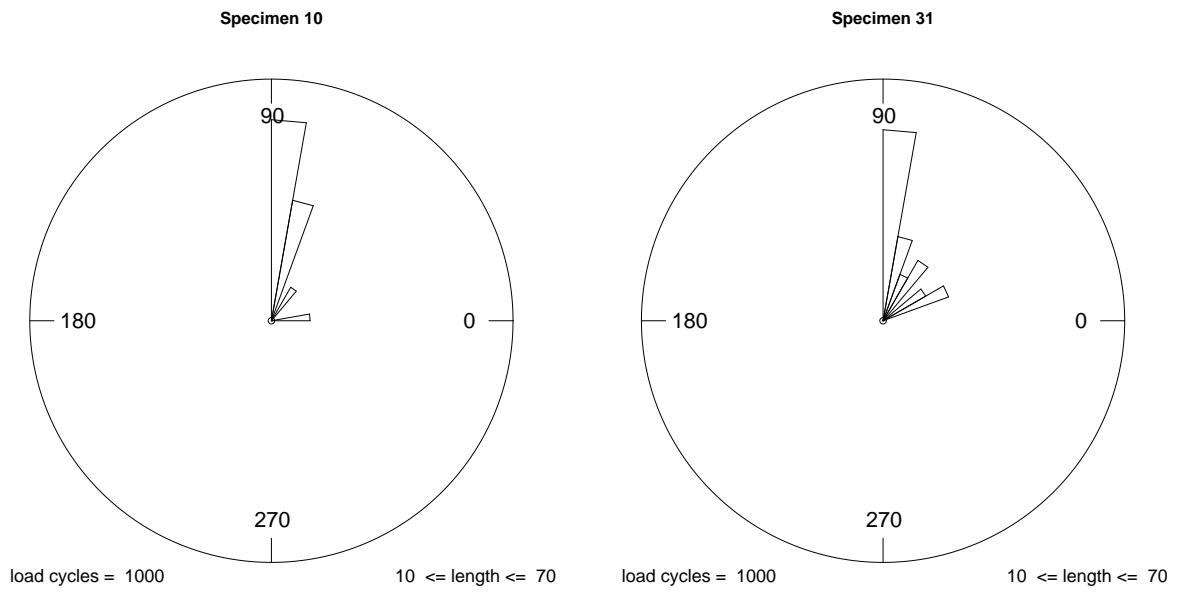


Figure 28: 1000 load cycles. Left: Specimen 10; Right: Specimen 31

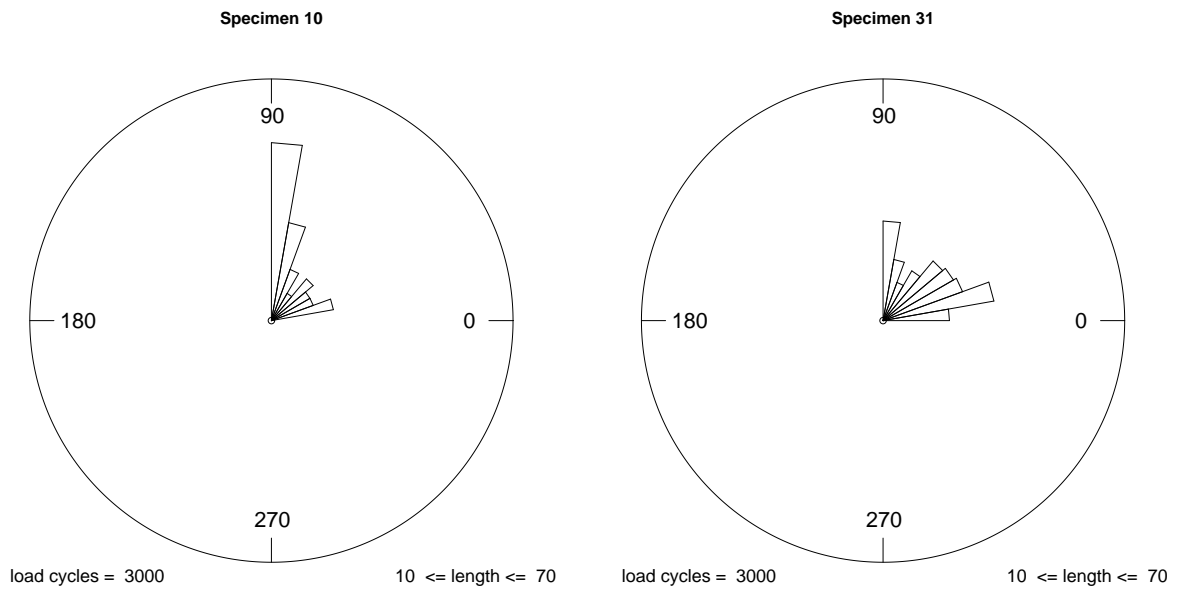


Figure 29: 3000 load cycles. Left: Specimen 10; Right: Specimen 31

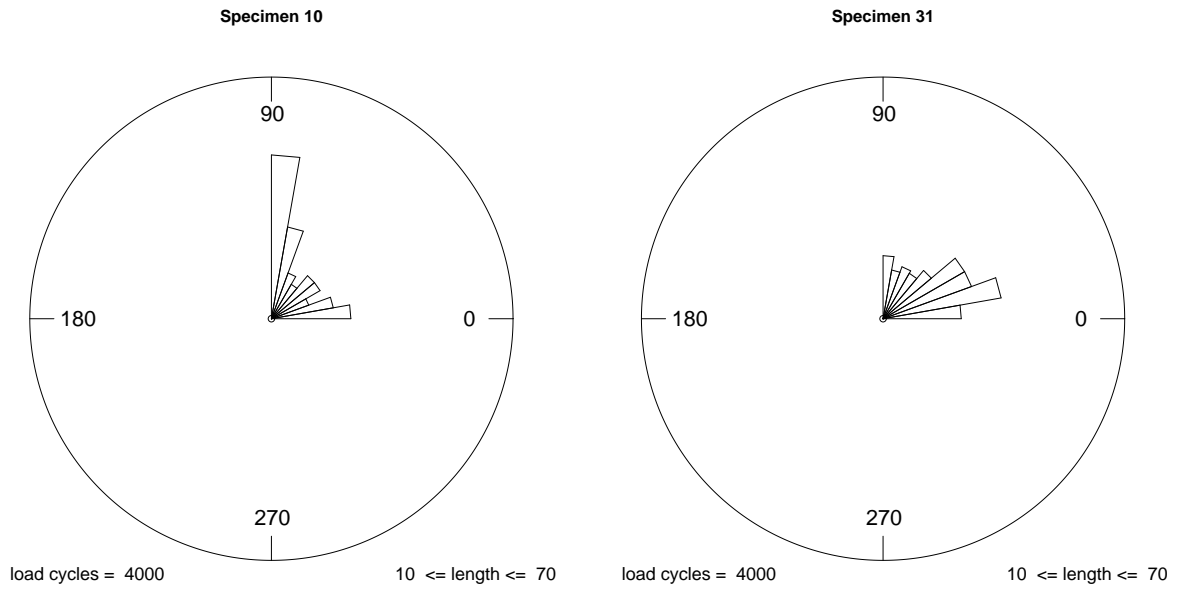


Figure 30: 4000 load cycles. Left: Specimen 10; Right: Specimen 31

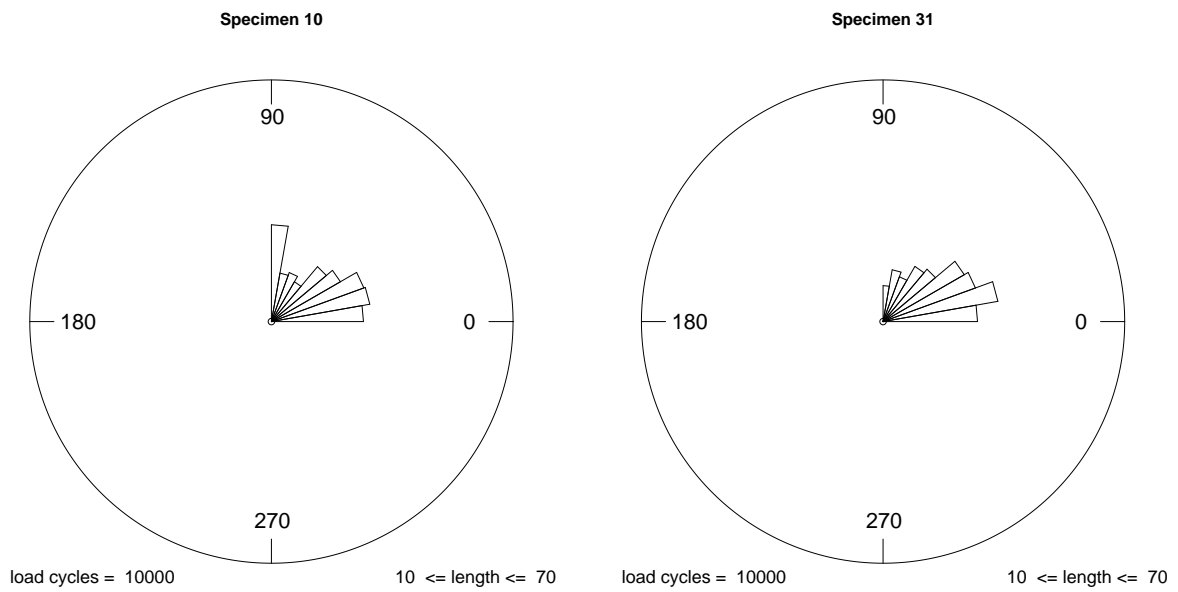


Figure 31: 10000 load cycles. Left: Specimen 10; Right: Specimen 31

A.2 Tables

Section 5.1: Graphical Representation

Table 14: Orientations of 76 turtles

Direction in degrees									
8	9	13	13	14	18	22	27	30	34
38	38	40	44	45	47	48	48	48	48
50	53	56	57	58	58	61	63	64	64
64	65	65	68	70	73	78	78	78	83
83	88	88	88	90	92	92	93	95	96
98	100	103	106	113	118	138	153	153	155
204	215	223	226	237	238	243	244	250	251
257	268	285	319	343	350				

Section 6.2: Crack Analysis of Specimen 10

Table 15: Number of cracks (length ≥ 10 pixels)

Specimen 10			
load cycles	number of cracks	load cycles	number of cracks
0	37	15000	316
1000	42	16000	314
2000	38	17000	338
3000	60	18000	388
4000	75	19000	432
5000	93	20000	440
6000	117	25000	434
7000	138	30000	494
8000	149	35000	886
9000	186	37000	724
10000	194	39000	770
11000	250	40000	727
12000	278	42000	350
13000	298	44000	582
14000	193		

Table 16: Maximum length after longest crack is omitted (in pixels)

Specimen 10			
load cycles	max. crack length	load cycles	max. crack length
0	32.90	15000	45.21
1000	70.91	16000	41.38
2000	51.14	17000	45.38
3000	35.66	18000	47.63
4000	35.66	19000	46.53
5000	35.49	20000	49.28
6000	37.31	25000	45.70
7000	35.66	30000	63.87
8000	35.07	35000	85.67
9000	35.66	37000	86.84
10000	34.66	39000	118.37
11000	37.97	40000	119.47
12000	36.87	42000	87.60
13000	37.04	44000	133.20
14000	34.66		

Table 17: Measures of location and dispersion per load cycle ($10 \leq \text{length} \leq 30$)

Specimen 10						
load cycles	number of cracks	circular mean direction	circular median direction	mean resultant length	circular variance	circular standard deviation
0	34	80.50°	84.90°	0.96	0.04	0.30
1000	35	81.56°	83.66°	0.98	0.02	0.22
2000	33	77.93°	84.29°	0.95	0.05	0.33
3000	55	69.97°	80.54°	0.91	0.09	0.44
4000	70	62.33°	78.30°	0.86	0.14	0.55
5000	88	49.94°	58.19°	0.84	0.16	0.58
6000	112	44.86°	37.37°	0.85	0.15	0.56
7000	132	41.23°	34.61°	0.86	0.14	0.54
8000	143	39.17°	30.96°	0.87	0.13	0.53
9000	181	34.51°	26.57°	0.88	0.12	0.50
10000	186	35.51°	27.06°	0.89	0.11	0.49
11000	242	33.59°	25.12°	0.90	0.10	0.46
12000	271	32.43°	23.96°	0.88	0.12	0.50
13000	288	31.14°	23.96°	0.90	0.10	0.46
14000	189	32.22°	26.57°	0.89	0.11	0.47
15000	309	31.04°	24.78°	0.90	0.10	0.45
16000	302	29.66°	23.96°	0.91	0.09	0.44
17000	327	30.14°	23.20°	0.90	0.10	0.45
18000	371	28.91°	23.96°	0.91	0.09	0.43
19000	415	28.74°	21.80°	0.91	0.09	0.44
20000	422	29.32°	23.80°	0.91	0.09	0.43
25000	415	29.18°	23.96°	0.92	0.08	0.42
30000	470	29.09°	22.91°	0.91	0.09	0.43
35000	812	28.43°	22.91°	0.92	0.08	0.40
37000	672	28.66°	23.96°	0.92	0.08	0.40
39000	707	28.30°	23.96°	0.92	0.08	0.40
40000	665	28.13°	23.20°	0.93	0.07	0.39
42000	326	27.97°	21.80°	0.92	0.08	0.42
44000	530	28.80°	21.80°	0.92	0.08	0.42

Table 18: Circular mean directions, grouped by different lengths

Specimen 10							
	<u>load cycles</u>						
	8000	9000	10000	11000	12000	13000	14000
$0 \leq \text{length} \leq 10$	22.88°	22.37°	22.25°	21.67°	21.65°	21.52°	21.26°
$\text{length} \geq 10$	40.29°	35.15°	36.29°	34.27°	32.60°	31.61°	32.60°
$\text{length} \geq 30$	68.27°	60.61°	54.95°	57.20°	40.09°	45.76°	52.99°
all cracks	23.71°	23.05°	22.96°	22.40°	22.30°	22.14°	21.84°
	<u>load cycles</u>						
	15000	16000	17000	18000	19000	20000	25000
$0 \leq \text{length} \leq 10$	22.08°	21.49°	20.97°	21.24°	21.71°	22.22°	21.87°
$\text{length} \geq 10$	31.34°	29.86°	30.16°	29.66°	29.19°	29.70°	29.51°
$\text{length} \geq 30$	46.55°	35.13°	30.67°	47.20°	40.18°	39.09°	37.45°
all cracks	22.67°	22.03°	21.57°	21.81°	22.26°	22.75°	22.44°
	<u>load cycles</u>						
	30000	35000	37000	39000	40000	42000	44000
$0 \leq \text{length} \leq 10$	20.79°	20.78°	20.61°	20.98°	20.53°	20.79°	20.08°
$\text{length} \geq 10$	29.37°	28.19°	28.54°	28.00°	27.54°	27.00°	27.87°
$\text{length} \geq 30$	35.18°	25.62°	26.92°	24.73°	21.24°	14.63°	18.65°
all cracks	21.49°	21.49°	21.33°	21.65°	21.17°	21.25°	20.72°

Table 19: Measures of location and dispersion per load cycle ($10 \leq \text{length} \leq 70$)

Specimen 10						
load cycles	number of cracks	circular mean direction	circular median direction	mean resultant length	circular variance	circular standard deviation
0	36	79.21°	84.90°	0.94	0.06	0.34
1000	39	81.52°	83.99°	0.98	0.02	0.22
2000	37	75.92°	84.29°	0.93	0.07	0.38
3000	59	70.56°	81.25°	0.91	0.09	0.44
4000	74	63.19°	79.19°	0.86	0.14	0.54
5000	92	51.00°	60.91°	0.84	0.16	0.58
6000	116	45.88°	39.24°	0.85	0.15	0.57
7000	137	42.65°	38.29°	0.86	0.14	0.55
8000	148	40.49°	32.01°	0.86	0.14	0.54
9000	185	35.29°	28.30°	0.88	0.12	0.51
10000	193	36.42°	28.61°	0.88	0.12	0.50
11000	249	34.33°	26.57°	0.89	0.11	0.47
12000	277	32.68°	23.96°	0.88	0.12	0.50
13000	297	31.64°	23.96°	0.90	0.10	0.46
14000	192	32.71°	26.57°	0.89	0.11	0.48
15000	315	31.40°	24.78°	0.90	0.10	0.46
16000	313	29.92°	23.96°	0.91	0.09	0.44
17000	337	30.21°	23.20°	0.90	0.10	0.45
18000	387	29.70°	23.96°	0.91	0.09	0.44
19000	431	29.21°	21.80°	0.91	0.09	0.44
20000	439	29.74°	23.96°	0.91	0.09	0.43
25000	433	29.55°	23.96°	0.91	0.09	0.43
30000	493	29.39°	23.20°	0.91	0.09	0.44
35000	883	28.24°	22.62°	0.92	0.08	0.40
37000	722	28.59°	23.73°	0.92	0.08	0.41
39000	767	28.04°	23.20°	0.92	0.08	0.40
40000	721	27.66°	22.62°	0.93	0.07	0.39
42000	347	27.12°	19.98°	0.92	0.08	0.41
44000	575	28.14°	21.80°	0.92	0.08	0.42

Section 6.3: Crack Analysis of Specimen 31

Table 20: Maximum length after longest crack is omitted (in pixels)

Specimen 31			
load cycles	max. length	load cycles	max. length
0	56.43	8000	56.70
1000	55.70	9000	82.01
2000	39.97	10000	80.25
3000	64.18	12000	79.91
4000	39.73	14000	102.33
5000	47.80	16000	116.33
6000	48.36	18000	213.28
7000	55.11		

Table 21: Measures of location and dispersion per load cycle ($10 \leq \text{length} \leq 30$)

Specimen 31						
load cycles	number of cracks	circular mean direction	circular median direction	mean resultant length	circular variance	circular standard deviation
0	30	82.75°	85.42°	0.97	0.03	0.23
1000	21	77.77°	83.66°	0.96	0.04	0.29
2000	37	52.70°	59.04°	0.84	0.16	0.59
3000	103	39.38°	32.47°	0.88	0.12	0.51
4000	185	30.55°	24.78°	0.91	0.09	0.42
5000	351	31.81°	26.57°	0.92	0.08	0.42
6000	373	30.14°	27.76°	0.93	0.07	0.38
7000	555	29.98°	24.78°	0.93	0.07	0.39
8000	715	29.23°	25.02°	0.93	0.07	0.39
9000	746	29.10°	26.57°	0.94	0.06	0.37
10000	866	28.33°	23.96°	0.93	0.07	0.37
12000	999	28.24°	23.96°	0.93	0.07	0.37
14000	1315	29.14°	24.78°	0.93	0.07	0.39
16000	1274	29.08°	23.96°	0.93	0.07	0.38
18000	1363	29.48°	24.78°	0.93	0.07	0.39

Table 22: Circular mean directions, grouped by different lengths

Specimen 31					
	load cycles				
	5000	6000	70000	8000	9000
$0 \leq \text{length} \leq 10$	20.25°	19.49°	19.65°	19.95°	19.60°
length ≥ 10	31.70°	29.88°	30.08°	28.95°	28.87°
length ≥ 30	29.43°	25.66°	31.55°	25.82°	26.27°
all cracks	21.12°	20.32°	20.57°	20.85°	20.55°
	load cycles				
	10000	12000	14000	16000	18000
$0 \leq \text{length} \leq 10$	19.84°	20.39°	20.46°	20.81°	20.91°
length ≥ 10	28.62°	28.19°	29.01°	29.06°	29.15°
length ≥ 30	31.64°	27.86°	28.16°	28.94°	27.62°
all cracks	20.79°	21.31°	21.62°	21.94°	22.04°

Table 23: Measures of location and dispersion per load cycle ($10 \leq \text{length} \leq 70$)

Specimen 31						
load cycles	number of cracks	circular mean direction	circular median direction	mean resultant length	circular variance	circular standard deviation
0	31	81.49°	85.24°	0.97	0.03	0.26
1000	24	75.16°	83.66°	0.94	0.06	0.34
2000	38	51.47°	52.02°	0.84	0.16	0.59
3000	106	39.00°	33.62°	0.88	0.12	0.51
4000	191	30.33°	24.44°	0.91	0.09	0.43
5000	367	31.59°	26.57°	0.92	0.08	0.42
6000	396	29.88°	26.57°	0.93	0.07	0.37
7000	595	30.01°	25.02°	0.93	0.07	0.39
8000	779	28.89°	24.78°	0.93	0.07	0.38
9000	809	28.83°	25.51°	0.94	0.06	0.36
10000	949	28.64°	24.23°	0.93	0.07	0.37
12000	1133	28.19°	23.96°	0.93	0.07	0.37
14000	1509	29.12°	24.78°	0.93	0.07	0.39
16000	1471	29.19°	24.44°	0.93	0.07	0.39
18000	1617	29.37°	24.62°	0.93	0.07	0.39

A.3 R-Codes

Figure 4: Value depends on choice of origin and sense of orientation

```
a <- seq(0,2*pi, length.out=100)
plot(cos(a),sin(a),xlim=c(-1,1),ylim=c(-1,1),type="l",lwd=2,xlab="",ylab="",axes=FALSE,asp=1)
arrows(0, 0, cos(pi/3), sin(pi/3), cex=1.1)
points(0,1, pch=3); points(1,0, pch=3); points(0,-1, pch=3); points(-1,0, pch=3)
text(0,0.9, "North", cex=1.75); text(0.85,0,"East",cex=1.75)
text(0,-0.9, "South", cex=1.75); text(-0.85,0,"West",cex=1.75)
legend(0.4, 1, "30° or 60°?", bty = "n", cex=1.75)
```

Figure 5: Orientations of 76 turtles

```
library(CircNNTSR) # An R package for the statistical analysis of circular data
data(turtles_radians) # Directions of turtles in radians
library(CircStats) # An R package needed to plot a circular raw data plot
par(mar=c(1.0, 1.5, 1.5, 1.5))
# Circular raw data plots:
circ.plot(turtles_radians, shrink=1.2)
legend(-0.225,-1.1, "(a)", bty = "n", cex=1.5)
circ.plot(turtles_radians, stack=TRUE, bins=120, shrink=1.2, dotsep=20)
legend(-0.225,-1.1, "(b)", bty = "n", cex=1.5)
```

Figure 6: Arithmetic mean of two directions

```
a <- seq(0,2*pi, length.out=100)
plot(cos(a),sin(a),xlim=c(-1.15,1.15),ylim=c(-1.15,1.15),type="l",lwd=2,xlab="",ylab="",axes=FALSE,asp=1)
arrows(0, 0, cos(pi/12), sin(pi/12), cex=1.1, lwd=2) # 15°
arrows(0, 0, cos(pi*23/12), sin(pi*23/12), cex=1.1, lwd=2) # 345°
arrows(0, 0, cos(pi), sin(pi), cex=1.1, lty=5) # 180°
text(1.1,0.3, "15°", cex=1.5)
text(1.15,-0.3, "345°", cex=1.5)
text(-1.15,0, "180°", cex=1.5)
```

Figures 7 and 8: Three directions

```
# 1. plot: showing three arrows (=directions)
# -----
a <- seq(0,2*pi, length.out=100)
plot(cos(a),sin(a),xlim=c(-1,1),ylim=c(-1,1),type="n",lwd=2,xlab="",ylab="",axes=FALSE,asp=1)
arrows(-0.5, 0, -0.5+cos(pi/4), sin(pi/4), cex=1.1, col=3) # North-East
arrows(-0.5, 0, -0.5+cos(7*pi/4), sin(7*pi/4), cex=1.1, col=4) # South-East
arrows(-0.5, 0, 0.5, 0, cex=1.1, col=8) # East
text(0.5,0.75, "North-East", cex=1.5); text(0.5,-0.75, "South-East", cex=1.5); text(0.65,0, "East", cex=1.5)
box()

# 2. plot: vector addition
# -----
```

```

a <- seq(0,2*pi, length.out=100)
plot(cos(a),sin(a),xlim=c(-1,1),ylim=c(-1,1),type="n",lwd=2,xlab="",ylab="",axes=FALSE,asp=1)
arrows(-1, 0, -0.5, 0.5, cex=1.1, lwd=1.5, col=3)
arrows(-0.5, 0.5, -0.5+sqrt(0.5), 0.5, cex=1.1, lwd=1.5, col=8)
arrows(-0.5+sqrt(1/2), 0.5, sqrt(0.5), 0, cex=1.1, lwd=1.5, col=4)
arrows(-1, 0, sqrt(0.5), 0, cex=1.1, lty=2, lwd=2.5, col=2)
text(0.5,-0.4, "resultant vector", cex=1.5, col=2)
arrows(0.4, -0.35, 0.4, -0.05, cex=0.25, length=0.1)
box()

# 3. plot: mean vector
# -----
a <- seq(0,2*pi, length.out=100)
plot(cos(a),sin(a),xlim=c(-1,1),ylim=c(-1,1),type="n",lwd=2,xlab="",ylab="",axes=FALSE,asp=1)
arrows(-1, 0, -0.5, 0.5, cex=1.1, lwd=1.5, col=3)
arrows(-0.5, 0.5, -0.5+sqrt(0.5), 0.5, cex=1.1, lwd=1.5, col=8)
arrows(-0.5+sqrt(1/2), 0.5, sqrt(0.5), 0, cex=1.1, lwd=1.5, col=4)
arrows(-1, 0, sqrt(0.5), 0, cex=1.1, lty=2, col=9)
arrows(-1, 0, -1+((1+sqrt(0.5))/3), 0, cex=1.1, lwd=2.5, col=2)
text(-0.75,-0.4, "mean vector", cex=1.5, col=2)
arrows(-0.75, -0.35, -0.75, -0.05, cex=0.25, length=0.1)
box()

# 4. plot: three directions plus mean vector
# -----
a <- seq(0,2*pi, length.out=100)
plot(cos(a),sin(a),xlim=c(-1,1),ylim=c(-1,1),type="l",lwd=2,xlab="",ylab="",axes=FALSE,asp=1)
arrows(0, 0, cos(pi/4), sin(pi/4), cex=1.1, col=3) # North-East
arrows(0, 0, cos(7*pi/4), sin(7*pi/4), cex=1.1, col=4) # South-East
arrows(0, 0, 1, 0, cex=1.1, col=8) # East
text(0.775,0.75, "45°", cex=1.25); text(0.75,-0.775, "315°", cex=1.25); text(1.05,0, "0°", cex=1.25)
arrows(0, 0, ((1+2*cos(pi/4))/3), 0, cex=1.1, lwd=3.5, col=2)
box()

```

Figure 9: Relation between Cartesian and polar coordinates

```

a <- seq(0,2*pi, length.out=100)
plot(cos(a),sin(a),xlim=c(-1,1),ylim=c(-1,1),type="l",lwd=2,xlab="x",ylab="y",asp=1,cex.lab=1.5,cex.axis=1.5)
abline(h=0, lty=3); abline(v=0, lty=3)
points(cos(pi/6), sin(pi/6), pch=19)
arrows(0, 0, cos(pi/6), sin(pi/6), lwd=2.5, length=0, col="green")
text(0.45,0.35, expression(r), cex=1.75, col="green")
arrows(cos(pi/6), 0, cos(pi/6), sin(pi/6), lwd=2.5, length=0, col="brown")
text(0.8,0.2, expression(y), cex=1.75, col="brown")
arrows(0, 0, cos(pi/6), 0, lwd=2.5, length=0, col="blue")
text(0.45,-0.1, expression(x), cex=1.75, col="blue")
text(0.25,0.075, expression(theta), cex=1.75)
text(1,0.6, expression('(x, y)'), cex=1.5)
text(1.025,0.475, expression(paste('(r, ', theta, ')')), cex=1.5)

```

Plotting rose diagrams

```

### -----
### GRAPHICAL REPRESENTATION
### Function that plots rose diagram with angles in [0°, 90°]:
### -----

library(CircStats) # package needed to plot circular raw data plot and rose diagram

graph.rep <- function(X, lc, min.l, max.l, bin.rose)
# Input: X ... 6xK matrix (containing length, size, x-/y-coordinates per load cycle),
#       lc ... number of load cycles
#       min.l ... minimum length of cracks to be included in analysis
#       max.l ... maximum length of cracks to be included in analysis
#       bin.rose ... number of bins in rose diagram
{
  X <- X[X["length",]>=min.l] # only cracks with length >= min.l
  X <- X[X["length",]<=max.l] # only cracks with length <= max.l
  n <- length(X["length",]) # number of cracks with min.l <= length <= max.l
  print(c("Number of cracks: ", n))

  diff.x <- X["End_x",] - X["Begin_x",] # difference x-coordinates
  diff.y <- X["End_y",] - X["Begin_y",] # difference y-coordinates
  diff.coord <- cbind(diff.x, diff.y) # combining diff.x & diff.y in one vector

  ### -----
  ### Calculate angles:
  ### -----
  # RADIANS:
  radian <- numeric(n) # empty vector to store radians
  for (i in (1:n)) {
    if (diff.x[i]==0 & diff.y[i]==0){radian[i] <- 0} # if x- and y-coordinate = 0 ---> radian=0
    else{radian[i] <- acos(diff.x[i]/sqrt(diff.x[i]^2+diff.y[i]^2))} # cos(theta) = adj/hyp

  for (i in (1:n)) # if angle is between pi/2 & pi, "reduce" it to be between 0 & pi/2
  # by reflecting it along the y-axis
  { if (radian[i]>pi/2){radian[i] <- radian[i]-2*(radian[i]-pi/2)} }

  par(mar=c(0.0, 0.0, 3.0, 1.0)) # margins of the plot
  ### -----
  ### ROSE DIAGRAM:
  ### -----
  rose.diag(radian, bins=bin.rose, main="Specimen 31", shrink=1.1)
  legend("bottomleft", cex=1.25, bty = "n", paste("load cycles = ", lc))
  # legend("bottomright", cex=1.25, bty = "n", paste("length >= ", min.l))
  legend("bottomright", cex=1.25, bty = "n", paste(min.l, " <= length <= ", max.l))
}

```

Calculating the measures of location and dispersion

```

### -----
### DESCRIPTIVE STATISTICS
### Function that calculates and prints summary statistics:
### -----
descr.summ.s31 <- function(X, min.l, max.l)
# Input: X ... 6xK matrix (containing length, size, x-/y-coordinates per load cycle),
#       min.l ... minimum length of cracks to be included in analysis
#       max.l ... maximum length of cracks to be included in analysis
{
  X <- X[X["length",]>=min.l]
  X <- X[X["length",]<=max.l]
  n <- length(X[1,])
  print(c("Number of cracks: ", n))
  print(c("Max. length: ", round(max(X[1,]),2)))

  diff.x <- X["End_x",] - X["Begin_x",]; diff.y <- X["End_y",] - X["Begin_y",]
  diff.coord <- cbind(diff.x, diff.y)

  ### -----
  ### Calculate angles:
  ### -----
  # RADIANS:
  radian <- numeric(n) # empty vector to store radians
  for (i in (1:n)) {
    if (diff.x[i]==0 & diff.y[i]==0){radian[i] <- 0} # if x- and y-coordinate = 0 ---> radian=0
    else{radian[i] <- acos(diff.x[i]/sqrt(diff.x[i]^2+diff.y[i]^2))} # cos(theta) = adj/hyp

  for (i in (1:n)) # if angle is between pi/2 & pi, "reduce" it to be between 0 & pi/2
    # by reflecting it along the y-axis
    { if (radian[i]>pi/2){radian[i] <- radian[i]-2*(radian[i]-pi/2)} }

  # Convert to DEGREES:
  degree <- radian*180/pi

  ### -----
  ### MEASURES OF LOCATION, CONCENTRATION AND DISPERSION:
  ### -----
  # Cartesian coordinates of center of mass:
  C.bar <- mean(cos(radian))
  S.bar <- mean(sin(radian))
  # Mean resultant length:
  R.bar <- sqrt(C.bar^2 + S.bar^2)
  # Mean direction:
  C <- n*C.bar
  S <- n*S.bar
  if(C>0 & S>=0){theta.bar <- atan(S/C)}
  if(C<0){theta.bar <- atan(S/C)+pi}
}

```

```

    if(C>=0 & S<0){theta.bar <- atan(S/C)+2*pi}
    if(C==0 & S>0){theta.bar <- pi/2}
    if(C==0 & S==0){theta.bar <- NA}
# Median direction:
    theta.tilde <- median(radian)
    theta.tilde*180/pi
# Resultant length:
    R <- n*R.bar
# Circular variance:
    V <- 1-R.bar
# Circular range:
    rad.sort <- sort(radian) # sort angles in ascending order
    T.i <- c(rad.sort[2:n]-rad.sort[1:(n-1)],2*pi+rad.sort[1]-rad.sort[n])
    w <- (2*pi-max(T.i))*180/pi
# Circular standard deviation:
    v <- sqrt(-2*log(R.bar))

### -----
### Print information:
### -----
    print(c("Mean resultant length:", round(R.bar, 2)))
    print(c("Mean direction:", round(theta.bar, 2), round(theta.bar*180/pi, 2)))
    print(c("Median direction:", round(theta.tilde, 2), round(theta.tilde*180/pi, 2)))
    print(c("Circular variance:", round(V, 2)))
    print(c("Circular standard deviation:", round(v, 2)))
}

```

Figure 23: Circular mean directions and 95% Wilcoxon confidence intervals for each specimen

```

# function to calculate and plot 95% Wilcoxon confidence intervals:
# -----
'wilcox.compare' <- function (x, y)
# Input:
# x ... list of orientations of the cracks present per time point in Specimen 10
# y ... list of orientations of the cracks present per time point in Specimen 31
{
    xL <- length(x) # 29 time points for Specimen 10
    yL <- length(y) # 15 time points for Specimen 31
    xwilcox <- NULL
    ywilcox <- NULL
    for(i in 1:xL){
        xwilcox <- cbind(xwilcox,wilcox.test(x[[i]],conf.int=T)$conf.int) }
    for(i in 1:yL){
        ywilcox <- cbind(ywilcox,wilcox.test(y[[i]],conf.int=T)$conf.int) }
    plot(-1,0,ylim=c(min(c(xwilcox[1,],ywilcox[1,])),
        max(c(xwilcox[2,],ywilcox[2,])+5)),xlim=c(1,19),
        ylab="Mean direction (in degrees)",xlab="Number of load cycles (x 1000)", , xaxt = "n")
}

```

```

axis(1, at=c(1:19), label=c(0:18))
t.s10 <- c(1:19)
segments(t.s10,xwilcox[1,],t.s10,xwilcox[2,], col="lightslategray")
t.s31 <- c(1:11, 13, 15, 17, 19)
segments(t.s31+0.1,ywilcox[1,],t.s31+0.1,ywilcox[2,], lty=1)
}

wilcox.compare(x[1:19], y)
points(mean.s10[1:19], pch=21, bg="grey85"); points(mean.s31, pch=16)
legend("top", c("Specimen 10", "Specimen 31"), pch=c(21,16), pt.bg=c("grey85", "black"),
      col=c("lightslategray", "black"), lty=c(1,1))

```

Table 13: P-values of the two-sample Wilcoxon test

```

p.values <- NULL
for(i in c(1:11)){ p.values[i] <- wilcox.test(x[[i]], y[[i]], paired=FALSE)$p.value}
p.values[12] <- wilcox.test(x[[13]], y[[12]], paired=FALSE)$p.value
p.values[13] <- wilcox.test(x[[15]], y[[13]], paired=FALSE)$p.value
p.values[14] <- wilcox.test(x[[17]], y[[14]], paired=FALSE)$p.value
p.values[15] <- wilcox.test(x[[19]], y[[15]], paired=FALSE)$p.value
round(p.values, 4)

```

B References

Besel, M. and Brückner-Foit, A. (2008). Surface damage evolution of engineering steel. *Fatigue & Fracture of Engineering Materials & Structures*, **31**, 885-891.

Fisher, N. I. (1993). *Statistical analysis of circular data*. Cambridge University Press, Cambridge.

Gunkel, C., Stepper, A., Müller, A. C. and Müller, Ch. H. (2011). Micro crack detection with Dijkstra's shortest path algorithm. To appear in *Machine Vision and Applications*. DOI: 10.1007/s00138-011-0324-1.

Jammalamadaka, S. R. and SenGupta, A. (2001). *Topics in circular statistics*. World Scientific Publishing, Singapore.

Mardia, K. V. and Jupp, P. E. (2000). *Directional Statistics*. Wiley, Chichester.

Müller, Ch. H., Gunkel, C. and Denecke, L. (2011). Statistical analysis of damage evolution with a new image tool. *Fatigue & Fracture of Engineering Materials & Structures*, **34**, 510–520.

R Development Core Team (2009). *R: A language and environment for statistical computing*. R Foundation for Statistical Computing, Vienna, Austria, <http://cran.r-project.org/>

Stephens, M. A. (1969). *Techniques for directional data*. Technical Report No. 150, Department of Statistics, Stanford University, Stanford, California, <http://statistics.stanford.edu/~ckirby/techreports/ONR/SOL%20NR%20150.pdf>. Retrieved: June 28, 2011.

Eidesstattliche Erklärung des Urhebers

Hiermit erkläre ich, dass ich die vorliegende Arbeit selbstständig verfasst und keine anderen als die angegebenen Quellen und Hilfsmittel benutzt sowie wörtliche und sinngemäße Zitate kenntlich gemacht habe.

Dortmund, den 21. Juli 2011

Unterschrift